Supporting information

to

Communication of Molecular Fluorophores with Other Photoluminescence Centres in

Carbon Dots

1. Isolated molecules

Table S1. Ground state singlet and triplet SCF energies of the molecules which served as a building block for interacting PAH/IPCA systems.

| System	Singlet (hartree)	Triplet (hartree)	Difference (kcal/mol)
A	-615.647158204	-615.566554634	-50.6
B	-648.858384211	-648.823295350	-22.0
C	-648.934446738	-648.882968585	-32.3
D	-798.209673698	-798.157501818	-32.7
E	-837.473553228	-837.450313949	-14.6
F	-837.542643360	-837.516961634	-16.1
G	-615.647158204	-615.566554634	-50.6
H	-644.885218730	-644.811668592	-46.2
J	-648.838982761	-648.847338725	5.2

The doping patterns in our modelled PAHs were selected based on a previous study, where the stability of various N-doped structures and the tuning of the UV spectrum with N-doping were investigated.[1] It was shown that out of four studied positions of double-doping with graphitic nitrogen, a Kekulé structure with graphitic nitrogens in a trans position separated by two carbon

atoms (NS = 2, system **B**; Figure S1a) demonstrated the lowest ground state (GS) relative energy. The graphitic-edge N-doped molecule (system **C**) corresponding to a Kekulé structure with two resonant structures each containing one Clar sextet (NS=4) exhibited one of the lowest GS relative energies among graphitic-edge N-doped molecules. It is worth noting that the graphitic doping leads to an increase of the π-electron density because each nitrogen contributes with two electrons to the delocalized π-electron system. As CDs usually possess O-containing functional groups on their surface and/or edges, some models were functionalized with either two oxo-groups (systems **D** and **E**) or one protonated carboxylic group (models **F** and **G**). In the system **E**, the graphitic-edge doping was replaced by two graphitic-core nitrogens in the same ring (referred as graphitic-N-core2 motif), as we only examined the Kekulé structures.

Importantly, the GSs of all presented structures in their geometrical minima were confirmed to be singlets, contrary to some other similar doubly doped structures being triplets in their GS (system **J** in Table S1, Figure S2) which were excluded from further analysis.
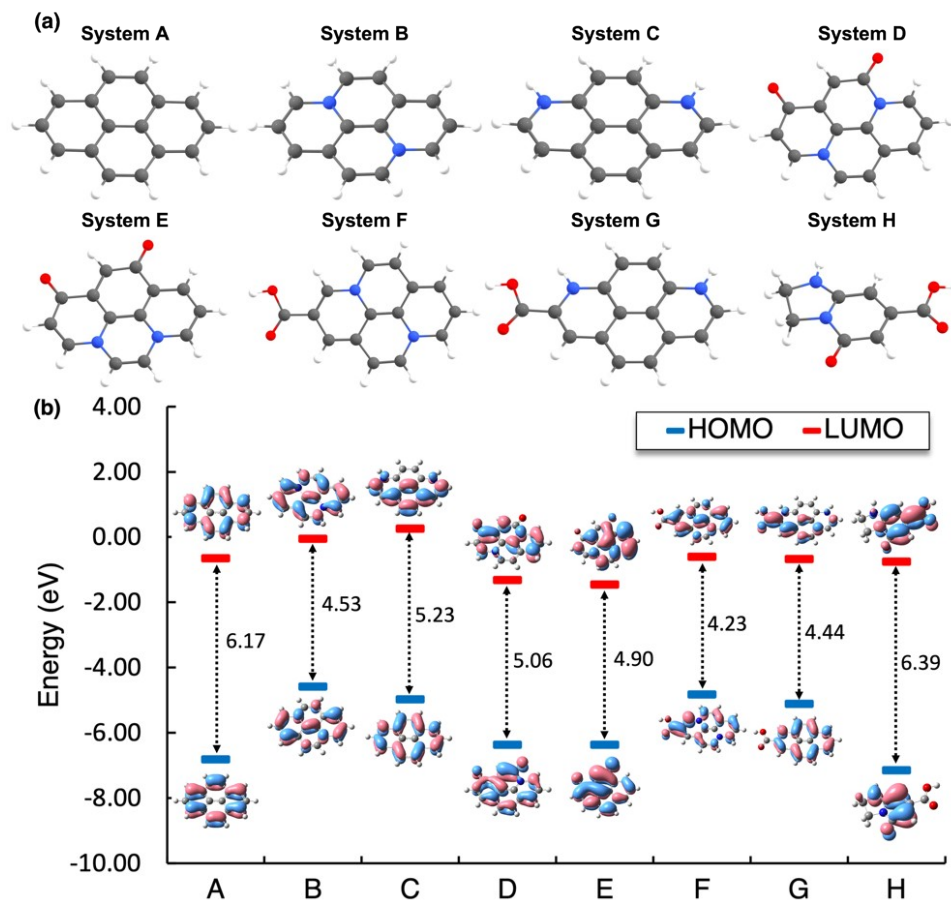
Figure S1. (a) Set of studied pyrene-like molecules (structures **A**–**G**) and molecular fluorophore IPCA (system **H**). (b) Frontier orbitals for the studied molecules calculated at the CAM-B3LYP-D3/def2TZVP/SMD level. The arrows indicate the HOMO-LUMO gaps in eV.
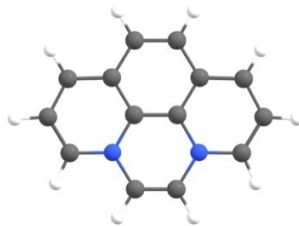
Figure S2. Graphitic-N-core2 model with nitrogens placed in para position in the same ring (system **J**).

Our calculations of optical properties are in line with a commonly observed redshift of the high-energy absorption bands due to the doping of PAHs (e.g., pyrene, model **A**) with graphitic nitrogens (see Figure S3 and Tables S2–S9). Generally, both absorption and emission maxima of structures with graphitic-N-edge doping motifs (models **C**, **G**) are less redshifted than in the corresponding systems with graphitic-N-core doping (systems **B**, **F**). On the other hand, the functionalization of the system **B** with oxo-groups (system **D**) caused blueshifts of both absorption and emission maxima. The shifts are qualitatively consistent with the calculated HOMO-LUMO gaps (Figure S1b). To predict the plausibility of the occurrence of low-lying intermolecular charge transfer (CT) transitions, the energies of frontier orbitals of IPCA were compared to those of the chosen PAHs. The HOMO of IPCA is the lowest in energy, however, five systems (**A–C**, **F–G**) demonstrate higher LUMO than IPCA. This suggests possible intermolecular CT excitations from pyrene-like molecules to IPCA. On the contrary, only the structures functionalized with oxo-groups have LUMO lower than IPCA, suggesting the possibility of CT excitations in the direction from IPCA to oxo-functionalized PAHs (systems **D**, **E**).

Experimental data measured in the gas phase showed that the first excited state of pyrene (**system** A) is a dark state characterized by an excitation energy of 369 nm and two dominant single excitations, HOMO–1 → LUMO and HOMO → LUMO+1 transitions.[2–4] The $S_1 \rightarrow S_0$ emission has the peak around 372 nm in the fluorescence spectrum.[1] $S_0 \rightarrow S_2$ excitation ($\lambda_{max} \approx 322$ nm) has a medium oscillator strength, and this state can be described as a combined HOMO → LUMO and HOMO–1 → LUMO+1 single excitation. Theoretically, multireference methods such as density functional theory/multireference configuration interaction (DFT/MRCI)[5] and strongly contracted n-electron valence state perturbation theory to second order (SC-NEVPT2)[6,7] describe these two excitations in good agreement with experiment.[4,8] However, it still poses a challenge for TD-DFT to correctly order these two states, as was demonstrated, e. g., for TD-B3LYP.[9–11] TD-CAM-

B3LYP/def2-TZVP calculations in gas provided the correct ordering of S_1 and S_2 states, where the first excitation energy was overestimated by 56 nm (308 nm) state and the second excitation energy overestimated by 16 nm (306 nm). In any case, these states are quasi-degenerate and, according to GMCQDPT calculations,[4] possess considerable multiconfiguration character. Overall, we can consider TD-CAM-B3LYP calculations an adequate level of theory for calculations of absorption spectra of bigger conjugated systems.

It was reported that in polar solvents like water, the forbidden vibronic bands in the vibrational structure of an electronic transition are much enhanced under the influence of the solvent polarity,[12] which can be supported by vibronic coupling between the S_1 and S_2 electronic states leading to an intensity borrowing effect, which is manifested as an enhancement of the weak $S_0 \rightarrow S_1$ transition intensity.[13] Thus, S_1 state being dark in gas may be visible in absorption spectra of pyrene in water. This behaviour was recorded in the experimental absorption spectrum with $\lambda_{max} \approx 360$ nm ($S_0 \rightarrow S_1$ excitation).[14] Similarly, $S_1 \rightarrow S_0$ emission peak ($\lambda_{max} \approx 415$ nm) is also clearly visible in the fluorescence spectra of pyrene in water.[13–15]

In our TD-CAM-B3LYP calculations using implicit solvation model, the first bright excited state (S_1) of pyrene is located at 313 nm ($f = 0.479$), which is reflected in the absorption spectra (Table S2, Figure S3a). This differs from the calculations in the gas phase,[1] where S_1 was a dark state with the excitation wavelength of 308 nm, followed by a bright $S_0 \rightarrow S_2$ (306 nm), dark $S_0 \rightarrow S_3$, and bright $S_0 \rightarrow S_4$ (244 nm, $f = 0.40$) transitions. Nevertheless, calculations of pyrene excitations with implicit solvent revealed similar trend as our calculations, i.e., bright S_1 and dark S_2 states.[16] Our calculations demonstrated the Kasha emission of light at 353 nm ($f = 1.12$), i.e., a region blue-shifted comparing with typically reported emissions in real CDs samples (Table S2).

According to the previous TD-DFT studies, doping with graphitic nitrogens redshifts the absorption maxima, while other types of nitrogen doping exhibits smaller effects.[17–19] TD-CAM-B3LYP calculations in gas phase[1] pointed on a big redshift of the $S_0 \rightarrow S_1$ transition (from 308 to 761 nm) when moving from pyrene to a graphitic-N-core model (system **B**), consistently with our calculations in implicit water ($\lambda_{max} = 751$ nm, $f = 0.00$, Figure S3b). The character of $S_0 \rightarrow S_1$ transition differs comparing to non-doped pyrene due to contribution of graphitic nitrogens with two electrons to the π-system. Thus, on contrary to non-doped pyrene, the

delocalization of π-orbitals over the entire structure is broken in the doped pyrene (see Table S3). The first bright excited singlet is S_3. The big energy gap of around 2 eV (209 nm) between S_3 and S_4 is consistent with the calculations in gas phase, which is caused by the inability of properly describing states with higher than single excitations with TD-CAM-B3LYP calculations.[1] The vertical emission energy from the S_1 state is significantly redshifted (1350 nm, f = 0.00). This might suggest that the deexcitation of this molecule is dominated by some non-radiative energy fluxes. It is also worth noting that deactivation via ISC is not plausible here, because of a relatively large S_1-T_2 energy gap (16.2 kcal/mol, Figure S4b).

The graphitic-N-edge doping pattern (system **C**) still causes a redshift of the $S_0 \rightarrow S_1$ transition (λ_{max} = 500 nm) compared to pyrene molecule, however, contrary to the graphitic-N-core doping (system **B**), this electronic transition is bright (f = 0.05). The S_1 state is slightly redshifted (by 13 nm) compared to the calculation in gas.[1] Additionally, all first four singlets S_1–S_4 are bright now (Figure S3c, Table S4). The $S_1 \rightarrow S_0$ emission is positioned at 771 nm (f = 0.08).

Functionalization of the graphitic-N-core model with two oxo-groups (system **D**) led to significant changes in the electronic structure, as the oxo-group is a chemical group with negative mesomeric effect, i.e., an electron-withdrawing group. Therefore, these surface groups can also contribute to the absorption of light (Table S5). Transitions to three lowest excited states S_1–S_3 are bright (Figure S3d) with the $S_0 \rightarrow S_1$ absorption band peaking at 447 nm (f = 0.31). As it is typical for conjugated molecules with very delocalized electronic density, the peak around 189 nm is a mixture of many energetically higher lying π-π* excitations. Although it could not be detected in the calculated absorption spectra, the presence of oxo-group brought n-π* excitations to the structure, as you can see for $S_0 \rightarrow S_4$ (Table S5). The $S_1 \rightarrow S_0$ emission wavelength is in an interesting region at 490 nm (f = 0.58).

The second model with oxo-groups, i.e., two graphitic nitrogens in the para position (system **E**), also exhibited redshift of $S_0 \rightarrow S_1$ transition (λ_{max} = 531 nm, f = 0.06) by 84 nm compared to that found for system **D** (Figure S3e). The character of this transition is slightly altered due to the position of the nitrogens on the cycle (Table S6). Interestingly, the presence of oxo-groups significantly changed the character of the $S_0 \rightarrow S_1$ transition compared to an non-functionalized molecule, where remarkably low-lying S_1 state (λ_{max} = 3351 nm) was reported in the gas phase calculations.[1] Again, dark n-π* transitions were observed for this system. The

$S_1 \rightarrow S_0$ emission of system **E** is redshifted (λ_{max} = 968 nm, f = 0.10) compared to the parent non-doped pyrene. A small singlet-triplet gap ΔE_{ST} gap of 1.0 kcal/mol between the S_1 and T_2 states suggested a plausibility of ISC (Figure S4e).

For both models with a single carboxylic group and N-doping (systems **F** and **G**), the $S_0 \rightarrow S_1$ excitations are redshifted compared to their non-functionalized counterparts. They are located at $\lambda_{max} \approx 837$ nm and $\lambda_{max} \approx 648$ nm for system **F** and **G**, respectively (Figures S3f, g), i.e., redshifted by 86 and 148 nm compared to their counterparts with no COOH groups. The redshift mainly originates in the involvement of electron densities of the –COOH group (Table S7, S8). Analogously as in the non-functionalized counterparts, S_1 is bright only for the doping pattern with graphitic-edge nitrogens (f = 0.087). Emissions are in the IR region, which is different compared to non-functionalized N-doped pyrene with graphitic-edge nitrogens (system **C**).

The first bright absorption transition of **IPCA** (system **H**) is $S_0 \rightarrow S_1$ at 342 nm (f = 0.16), the $S_1 \rightarrow S_0$ emission maximum is shifted to 435 nm (f = 0.23), and both have π-π* character (Figures S3h, Table S9). These results are consistent with our previous work using the same level of theory,[20] where the $S_0 \rightarrow S_1$ and $S_1 \rightarrow S_0$ transitions were predicted to be at 341 nm (f = 0.16) and 439 nm (f = 0.23), respectively. The consistency is also preserved by the dark $S_0 \rightarrow S_{2,3}$ excitations with n-π* character.

To summarize, we confirmed the commonly accepted understanding that the doping of the polyaromatic molecules with graphitic nitrogens causes redshifts of the long wavelength absorption bands. Out of three probed doping positions, the graphitic-N-edge doping appears to be the most interesting, as both absorptions and emissions are blue-shifted more than in systems with graphitic-N-core doping. On the other hand, the functionalization of the system **B** with oxo-groups (system **D**) caused blueshifts of both absorption and emission.
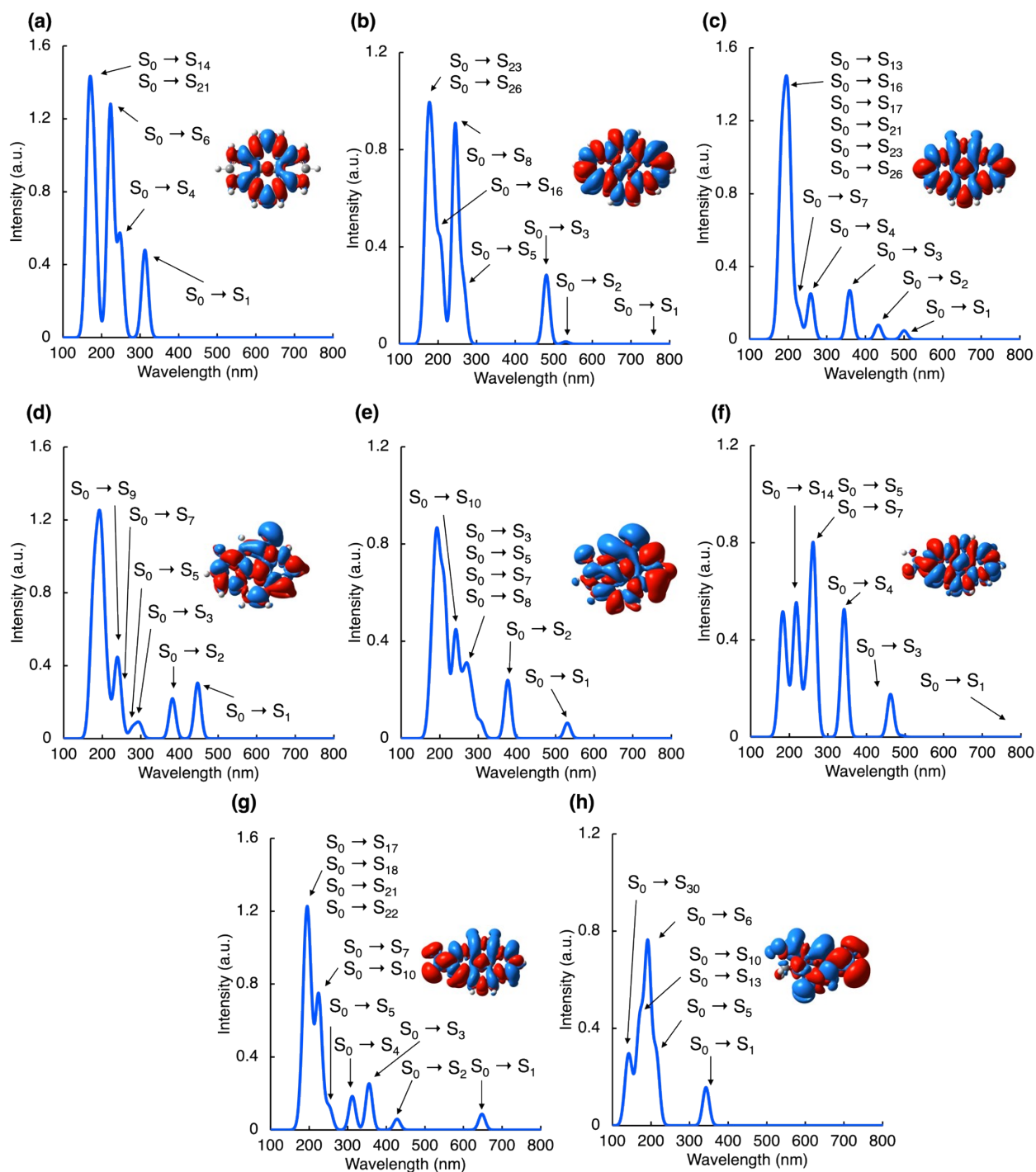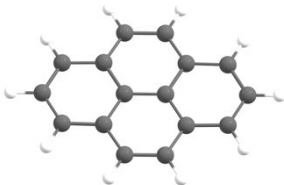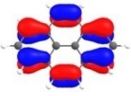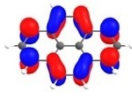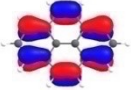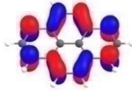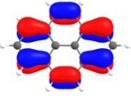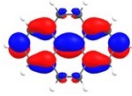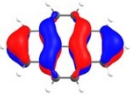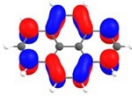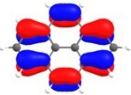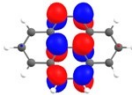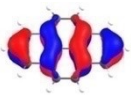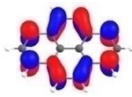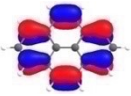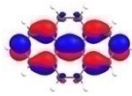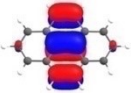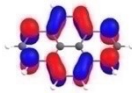
Figure S3. Absorption spectra of the PAHs (systems **A**–**G** in Figure S1) and IPCA (system **H** in Figure S1), which were used as a building block for the models of interaction systems of PAH/IPCA. For each spectrum, line spectra (excitation energy of 30 lowest singlet states with different oscillator strengths) were convoluted by a Gaussian function assuming the inhomogeneous broadening of peaks with $\sigma = 20$ nm. Insets: EDD plots for the $S_0 \rightarrow S_1$ transition (red/blue regions indicate increase/decrease of the electron density upon the excitation).
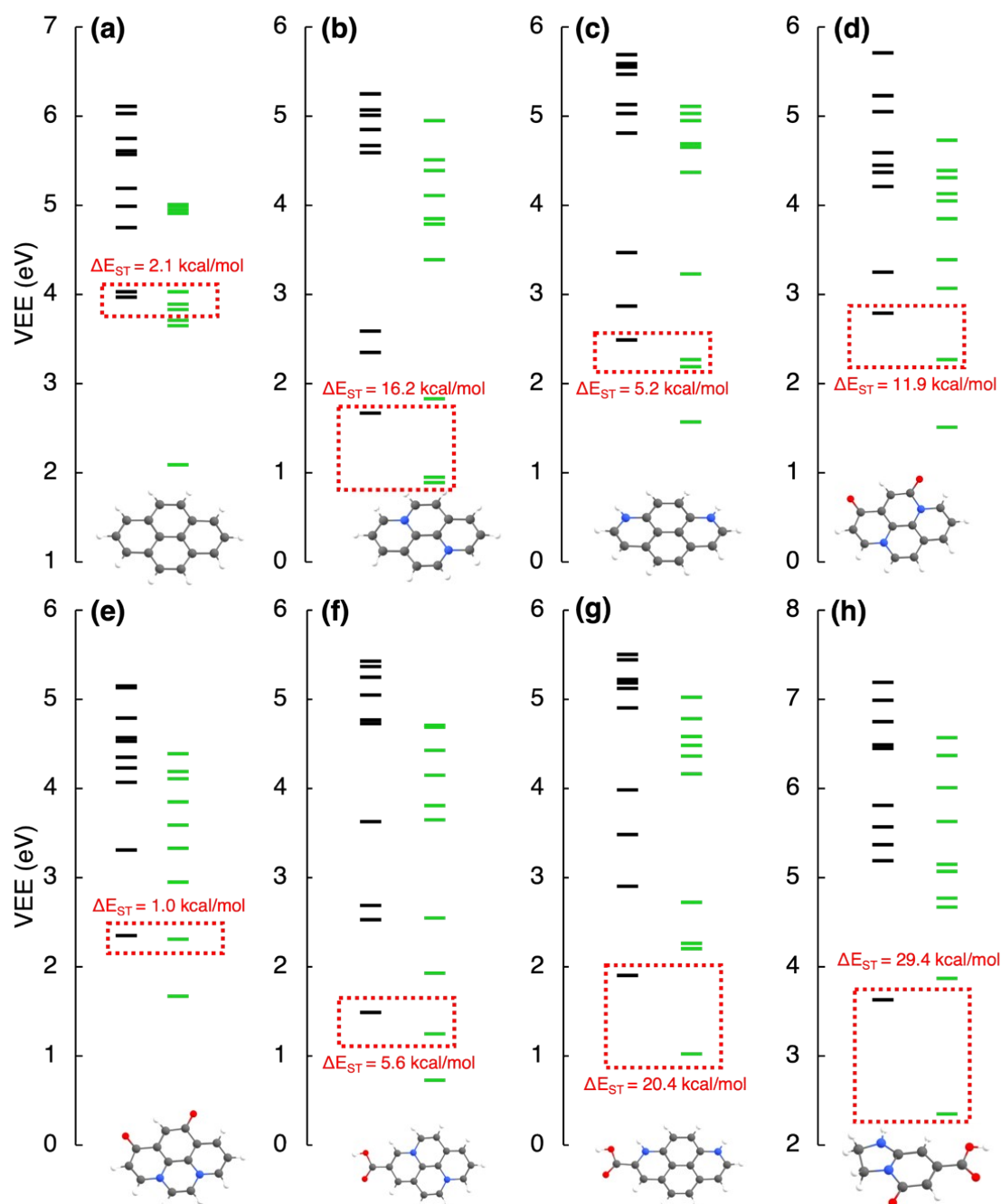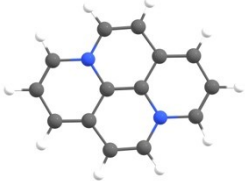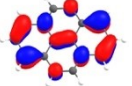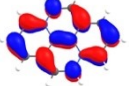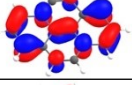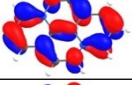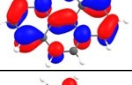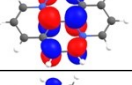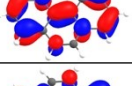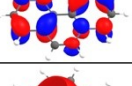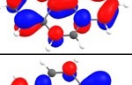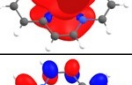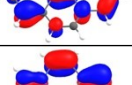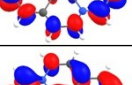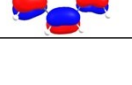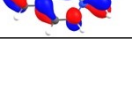
Figure S4. (a-h) Vertical excitation energies (VEE, in eV) of ten lowest singlet (black) and triplet (green) excited states for eight structures, which were used as a building block for the models of interaction systems of PAH/IPCA. Displayed values of ΔE_{ST} represent the vertical singlet-triplet energy gaps.
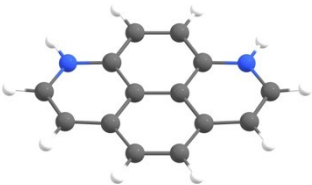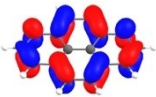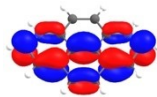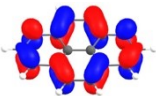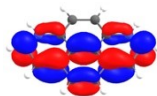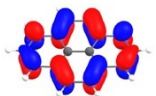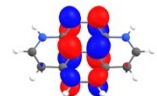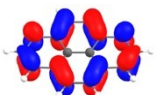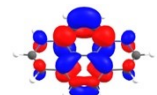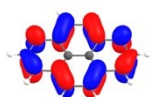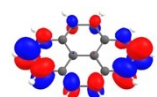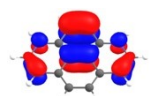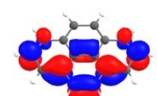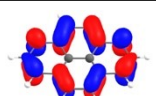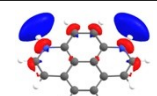
Table S2. NTO orbitals (only those with weight > 0.10 are shown; the isocontour value is 0.04 au), vertical excitation energies (VEEs, or vertical emission energy for the first row in the table) displayed for five lowest excited states for **system A**.
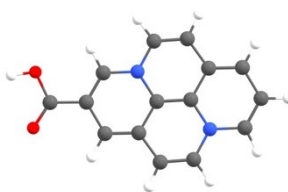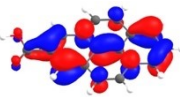

NTO (weight)	Hole	Electron	VEE (nm)	Oscillator strength
S_1 Emission			353	1.120
S_1 (0.92)			313	0.479
S_2 (0.57)			308	0.002
S_2 (0.41)				
S_3 (0.95)			261	0.000
S_4 (0.58)			248	0.556
S_4 (0.42)				
S_5 (0.92)			239	0.000
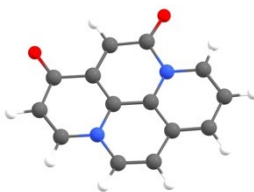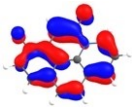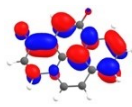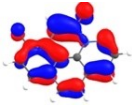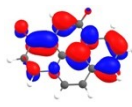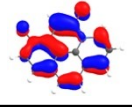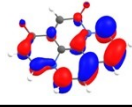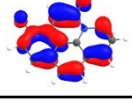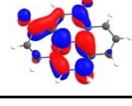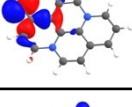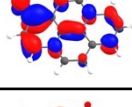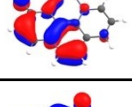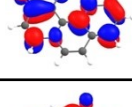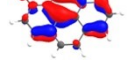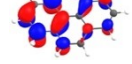
Table S3. NTO orbitals (only those with weight > 0.10 are shown; the isocontour value is 0.04 au), vertical excitation energies (VEEs, or vertical emission energy for the first row in the table) displayed for five lowest excited states for **system B**.
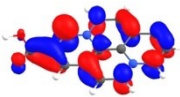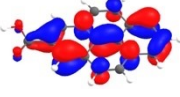

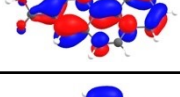| NTO (weight)	Hole	Electron	VEE (nm)	Oscillator strength
S_1 Emission			1350	0.000
S_1 (0.99)			751	0.000
S_2 (0.98)			531	0.010
S_3 (0.99)			481	0.285
S_4 (0.99)			271	0.010
S_5 (0.65)			266	0.229
S_5 (0.33)				

Table S4. NTO orbitals (only those with weight > 0.10 are shown; the isocontour value is 0.04 au), vertical excitation energies (VEEs, or vertical emission energy for the first row in the table) displayed for five lowest excited states for **system C**.
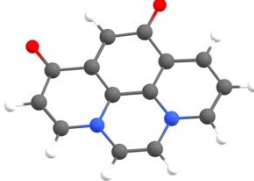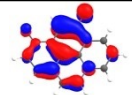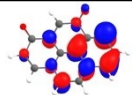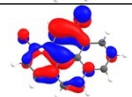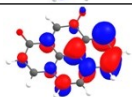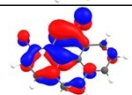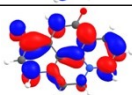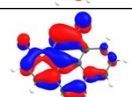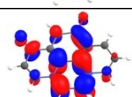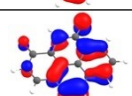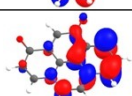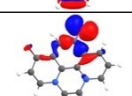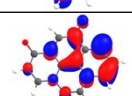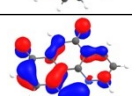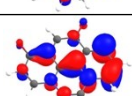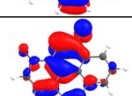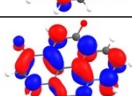
NTO (weight)	Hole	Electron	VEE (nm)	Oscillator strength
S_1 Emission			771	0.080
S_1 (0.99)			500	0.049
S_2 (0.97)			433	0.079
S_3 (0.98)			359	0.270
S_4 (0.84)			258	0.251
S_4 (0.10)				
S_5 (0.95)			247	0.000

Table S5. NTO orbitals (only those with weight > 0.10 are shown; the isocontour value is 0.04 au), vertical excitation energies (VEEs, or vertical emission energy for the first row in the table) displayed for five lowest excited states for **system D**.
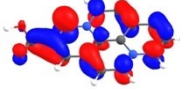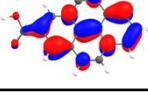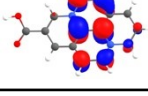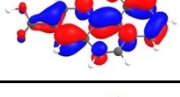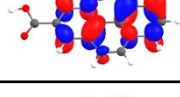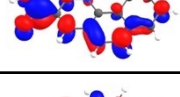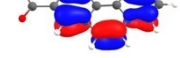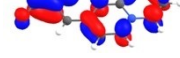
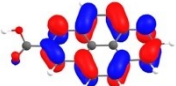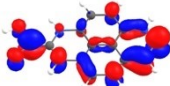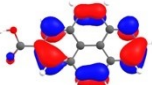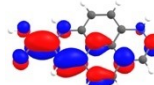| NTO (weight)	Hole	Electron	VEE (nm)	Oscillator strength
S_1 Emission			490	0.583
S_1 (0.99)			447	0.305
S_2 (0.97)			382	0.220
S_3 (0.94)			296	0.081
S_4 (0.99)			284	0.000
S_5 (0.58)			279	0.055
S_5 (0.41)				
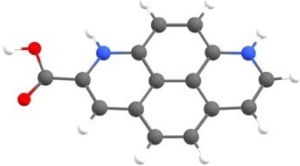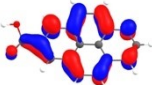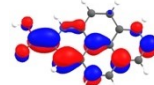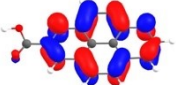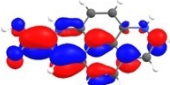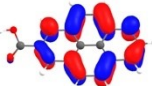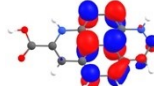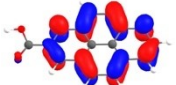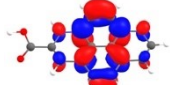
Table S6. NTO orbitals (only those with weight > 0.10 are shown; the isocontour value is 0.04 au), vertical excitation energies (VEEs, or vertical emission energy for the first row in the table) displayed for five lowest excited states for **system E**.

NTO (weight)	Hole	Electron	VEE (nm)	Oscillator strength
S_1 Emission			968	0.100
S_1 (1.00)			531	0.064
S_2 (0.96)			376	0.240
S_3 (0.86)			306	0.065
S_3 (0.13)				
S_4 (0.99)			294	0.000
S_5 (0.83)			286	0.115
S_5 (0.16)				
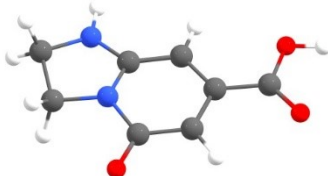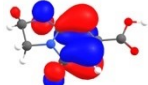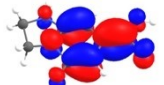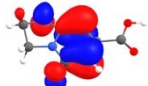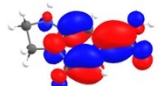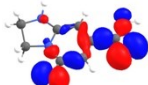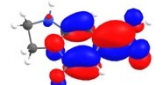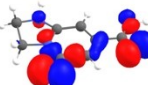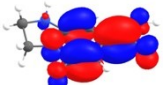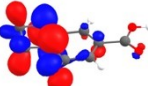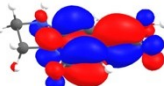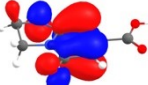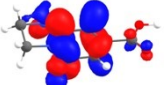
Table S7. NTO orbitals (only those with weight > 0.10 are shown; the isocontour value is 0.04 au), vertical excitation energies (VEEs, or vertical emission energy for the first row in the table) displayed for five lowest excited states for **system F**.

NTO (weight)	Hole	Electron	VEE (nm)	Oscillator strength
S_1 Emission			1587	0.016
S_1 (0.99)			837	0.018
S_2 (0.98)			490	0.007
S_3 (0.99)			462	0.176
S_4 (0.96)			342	0.526
S_5 (0.91)			262	0.758

Table S8. NTO orbitals (only those with weight > 0.10 are shown; the isocontour value is 0.04 au), vertical excitati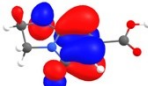on energies (VEEs, or vertical emission energy for the first row in the table) displayed for five lowest excited states for **system G**.

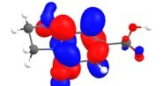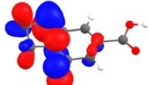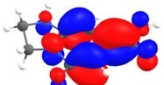| NTO (weight)	Hole	Electron	VEE (nm)	Oscillator strength
S_1 Emission			1434	0.142
S_1 (0.99)			648	0.087
S_2 (0.97)			428	0.060
S_3 (0.98)			355	0.254
S_4 (0.94)			312	0.185
S_5 (0.91)			253	0.108

Table S9. NTO orbitals (only those with weight > 0.10 are shown; the isocontour value is 0.04 au), vertical excitation energies (VEEs, or vertical emission energy for the first row in the table) displayed for five lowest excited states for **system H**.

| NTO (weight)	Hole	Electron	VEE (nm)	Oscillator strength
S_1 Emission			435	0.231
S_1 (0.99)			342	0.157
S_2 (0.93)			240	0.000
S_3 (0.91)			231	0.000
S_4 (0.87)			223	0.001
S_4 (0.12)				
S_5 (0.83)			214	0.285
S_5 (0.16)				

2. PAH/IPCA systems
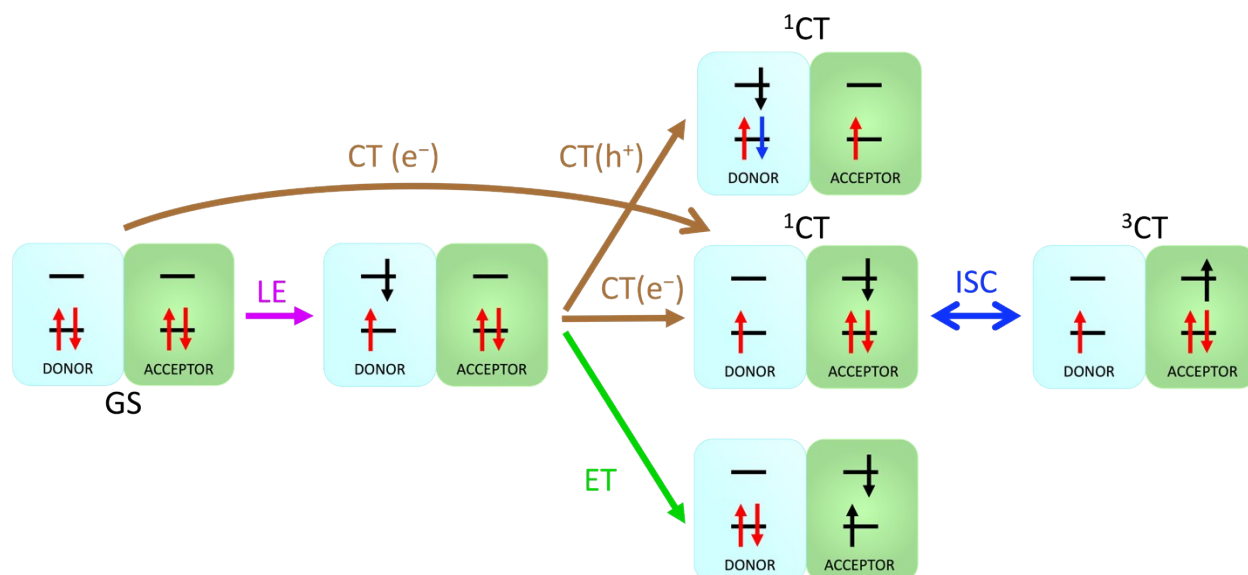
Figure S5. Scheme displaying charge and energy transfer processes occurring in the studied models upon excitation. LE represents local excitation, CT (e^-/h^+) charge (electron/hole) transfer, ET energy transfer, ISC intersystem crossing.

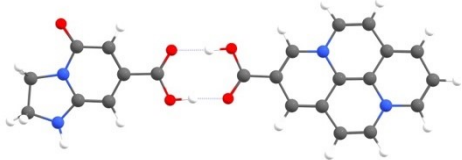**Table S10.** Ground state singlet and triplet SCF energies of the interacting PAH/IPCA model systems.

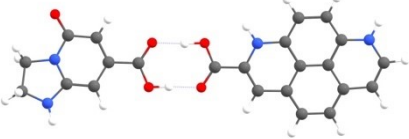| System	Singlet (hartree)	Triplet (hartree)	Difference (kcal/mol)
COOH_core	-1482.37852879	-1482.35736110	-13.3
COOH_edge	-1482.44742522	-1482.42395688	-14.7
Stacked_core	-1293.76499051	-1293.73577477	-18.3
Stacked_edge	-1293.84010272	-1293.80751019	-20.5
Oxo_stacked1_a	-1443.11634108	-1443.06467584	-32.4
Oxo_stacked1_b	-1443.11773764	-1443.06508889	-33.0
Oxo_stacked_2_a	-1443.08963697	-1443.05240349	-23.4
Oxo_stacked_2_b	-1443.09856045	-1443.05332302	-28.4
Ester1_core	-1292.53198325	-1292.49690511	-22.0
Ester1_edge	-1292.60999006	-1292.57964801	-19.0
Amide1_core	-1272.66707977	-1272.63154650	-22.3
Amide1_edge	-1272.74473104	-1272.69119770	-33.6
Amide2_core	-1272.67001131	-1272.63496488	-22.0
Amide2_edge	-1272.74379786	-1272.69220812	-32.4
Amide3_core	-1272.67020628	-1272.65015632	-12.6
Amide3_edge	-1272.74787566	-1272.72132957	-16.7
Fused	-1180.71730194	-1180.64432638	-45.8
Fused_core	-1213.92799900	-1213.89947425	-17.9
Fused_edge	-1213.97814168	-1213.95245646	-16.1
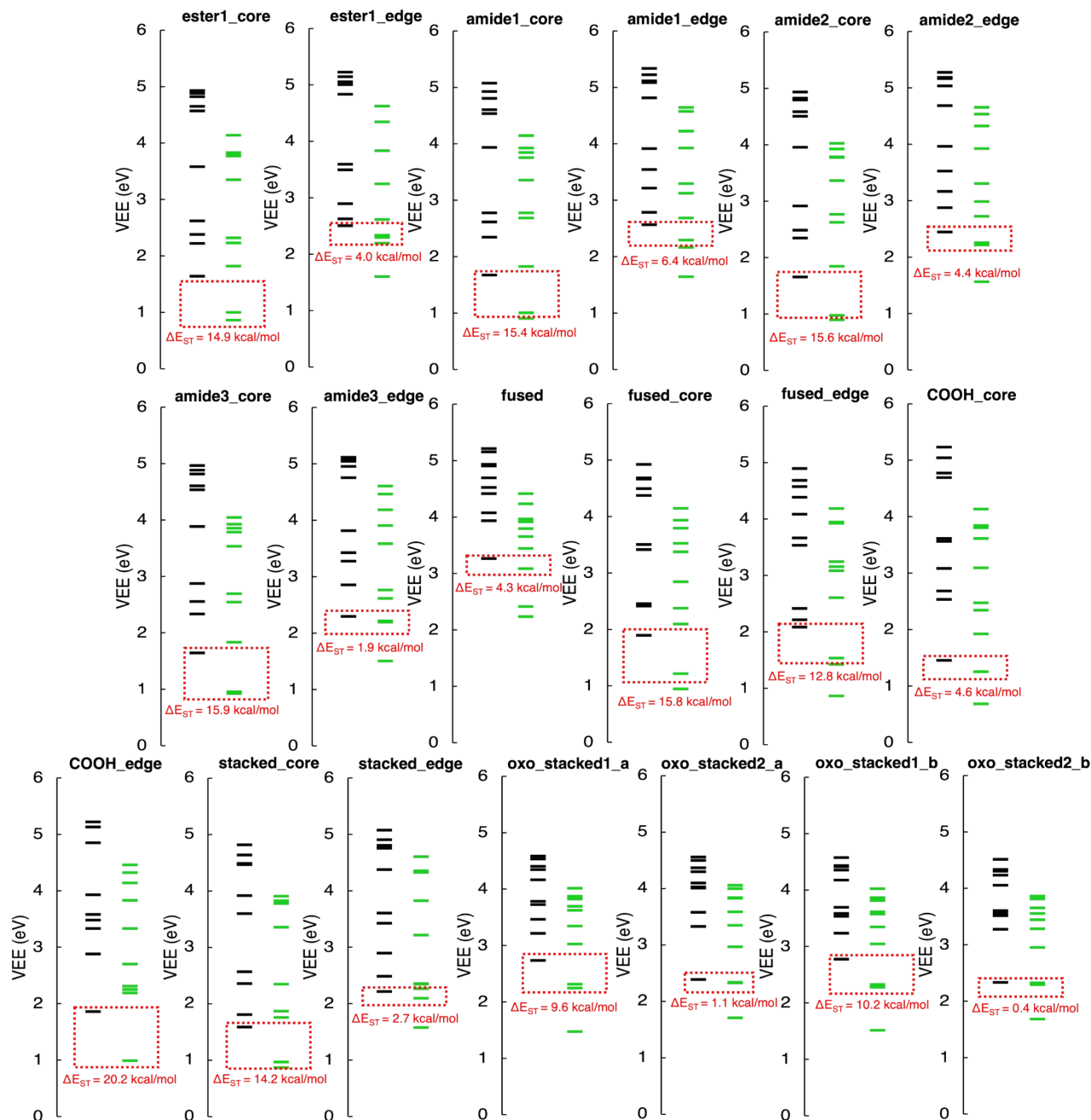
Figure S6. (a-h) Vertical excitation energies (VEE, in eV) to ten lowest singlets (black) and triplets (green) for our models of interaction systems of PAH/IPCA. Displayed values of ΔE_{ST} represent singlet-triplet energy gaps potentially interesting for ISC.
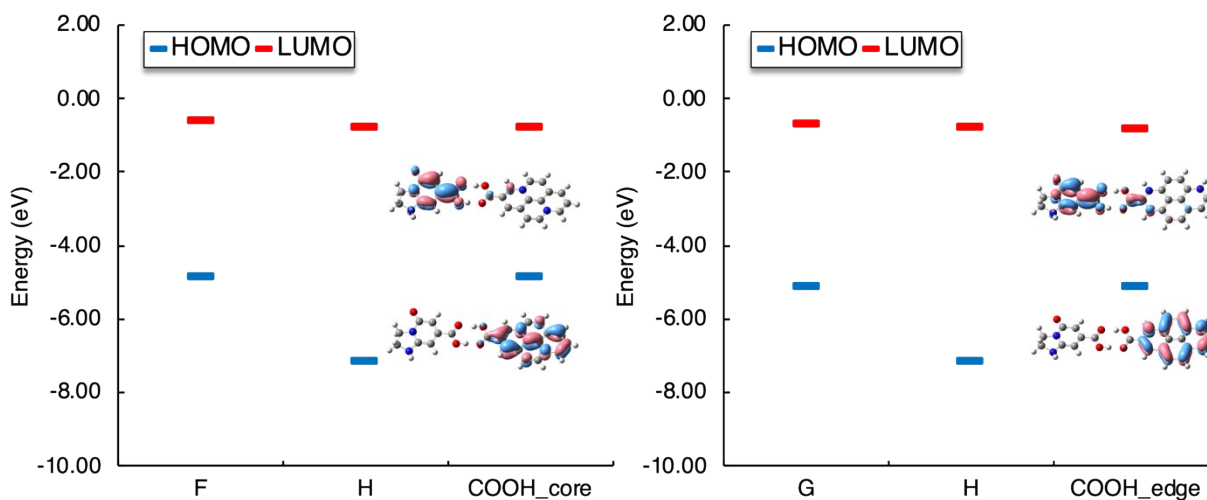
3. Hydrogen-bonded quasi-planar complexes

Table S11. NTO orbitals (only those with weight > 0.10 are shown; the isocontour value is 0.04 au), vertical excitation energies (VEEs, or vertical emission energy for the first row in the table) and the calculated CT distance[21,22] displayed for electronic over 280 nm for the **COOH_core** model.

NTO (weight)	Hole	Electron	VEE (nm)	Oscillator strength	D_{CT} (Å)
S_1 Emission			1640	0.023	
S_1 (0.99)			846	0.027	1.13
S_2 (0.98)			487	0.009	0.68
S_3 (0.99)			461	0.172	1.13
S_4 (1.00)			401	0.026	9.91
S_5 (0.97)			347	0.599	3.02
S_6 (0.99)			342	0.161	1.82

Table S12. NTO orbitals (only those with weight > 0.10 are shown; the isocontour value is 0.04 au), vertical excitation energies (VEEs, or vertical emission energy for the first row in the table) and the calculated CT distance[21,22] displayed for electronic over 280 nm for **COOH_edge** model.

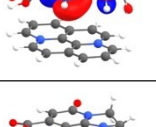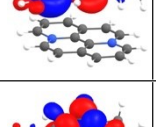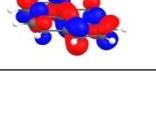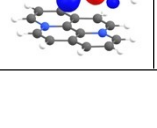| NTO (weight)	Hole	Electron	VEE (nm)	Oscillator strength	D_{CT} (Å)
S_1 Emission			1547	0.160	
S_1 (0.99)			660	0.103	2.37
S_2 (0.97)			428	0.057	0.23
S_3 (1.00)			371	0.002	10.05
S_4 (0.98)			355	0.273	0.35
S_5 (0.99)			345	0.148	1.87
S_6 (0.94)			314	0.193	1.38
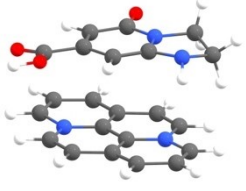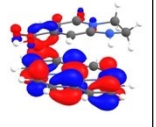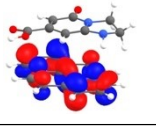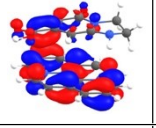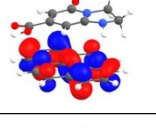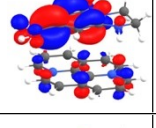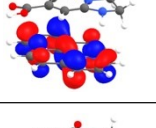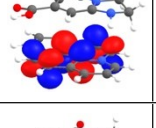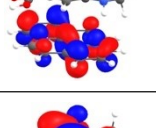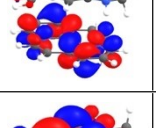
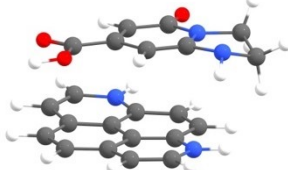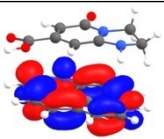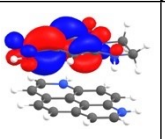**Figure S7.** HOMO and LUMO orbitals of the studied systems calculated with CAM-B3LYP-D3/def2-TZVP/SMD calculations.
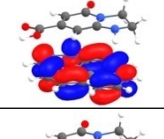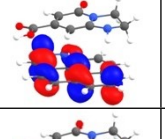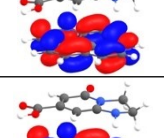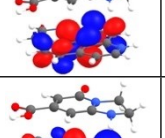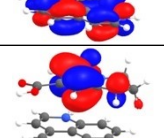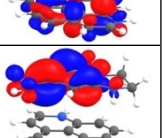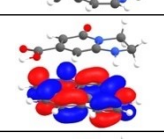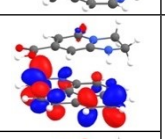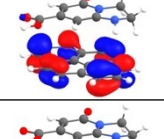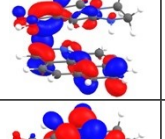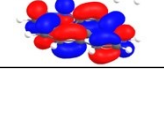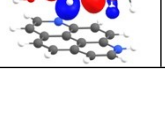
4. Stacked complexes

Table S13. NTO orbitals (only those with weight > 0.10 are shown; the isocontour value is 0.04 au), vertical excitation energies (VEEs, or vertical emission energy for the first row in the table) and the calculated CT distance[21,22] displayed for electronic over 280 nm for **stacked_core** model.

NTO (weight)	Hole	Electron	VEE (nm)	Oscillator strength	D_{CT} (Å)
S_1 Emission			1512	0.001	
S_1 (0.99)			782	0.000	1.33
S_2 (1.00)			688	0.002	3.01
S_3 (0.98)			526	0.007	0.05
S_4 (0.99)			483	0.220	0.19
S_5 (0.98)			345	0.097	1.83
S_6 (1.00)			317	0.004	3.39

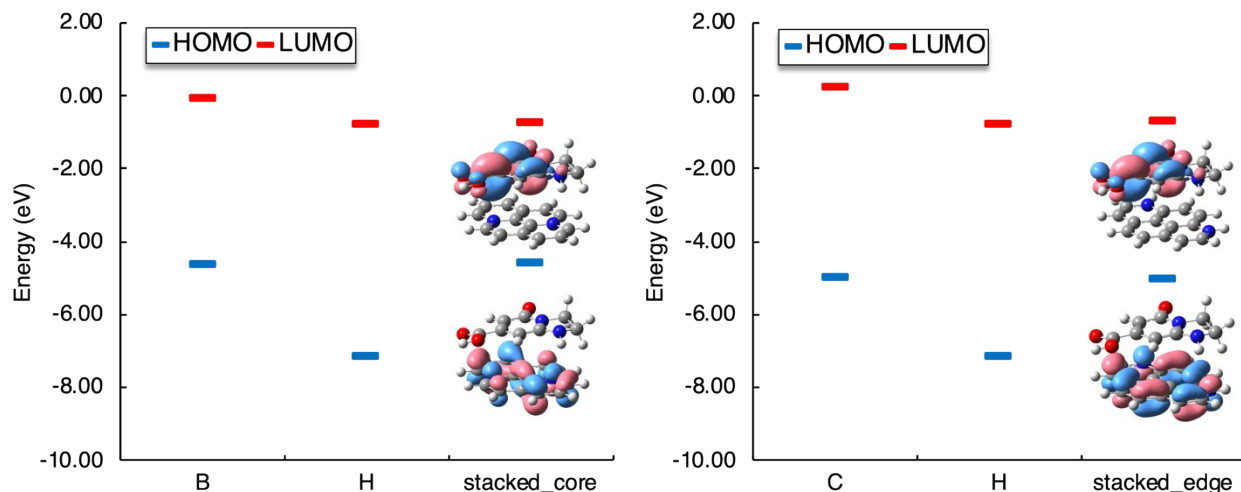**Table S14.** NTO orbitals (only those with weight > 0.10 are shown; the isocontour value is 0.04 au), vertical excitation energies (VEEs, or vertical emission energy for the first row in the table) and the calculated CT distance[21,22] displayed for electronic over 280 nm for **stacked_edge** model.

NTO (weight)	Hole	Electron	VEE (nm)	Oscillator strength	D_{CT} (Å)
S_1 Emission					
S_1 (1.00)			558	0.021	3.48
S_2 (0.99)			497	0.041	0.97
S_3 (0.97)			427	0.059	0.09
S_4 (0.88)			362	0.105	0.57
S_4 (0.11)					
S_5 (0.88)			343	0.210	1.62
S_5 (0.10)					
S_6 (0.99)			283	0.005	3.35

Figure S8. HOMO and LUMO orbitals of the studied systems calculated with CAM-B3LYP-D3/def2-TZVP/SMD calculations.

Note regarding Figure 4d:

For the **stacked_edge** model, the calculated vertical emission energy for the $S_1 \rightarrow S_0$ transition was 0.54 eV and –0.28 eV using the LR and cLR approaches, respectively. The wave-function stability test was performed, and it was found out that the wavefunction had an RHF$\rightarrow$UHF instability in the GS energy calculation at the excited state geometry indicating the vicinity of S_0 and S_1 energy levels, which was also confirmed by spin-flip TD-DFT (SF-TD-DFT)[23] calculations at the BHHLYP/def2-TZVP/SMD level of theory with GAMESS,[24] version 2022 (R1) (see Table S15). As the solvent polarization effects are significant in the **stacked_edge** model, the negative cLR emission energy is an artifact of cLR-TD-DFT calculation in this case.
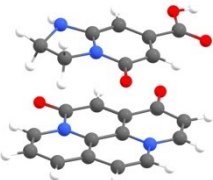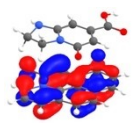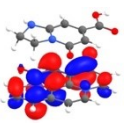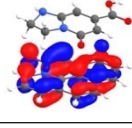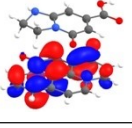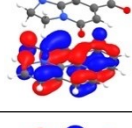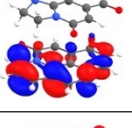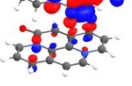
Table S15. TD-DFT and SF-TD-DFT vertical excitation energies (eV) and the S^2 values of the S_1 state (in parentheses) of **stacked_edge** model obtained using the BHHLYP and CAM-B3LYP methods in combination with the def2-TZVP basis set and the SMD solvation model (solvent=water).

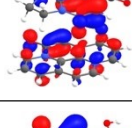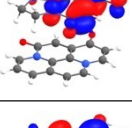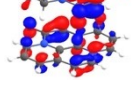| Geometry	gas phase		water		water	
	TD-BHHLYP	SF-TD-BHHLYP (S^2)	TD-BHHLYP	SF-TD-BHHLYP (S^2)	TD-CAM-B3LYP	SF-TD-CAM-B3LYP (S^2)
GS	2.65	2.68 (0.29)	2.28	1.39 (0.68)	2.29	1.53 (0.82)
S_1	1.22	1.49 (0.39)	0.97	0.19 (0.81)	1.02	0.37 (0.87)

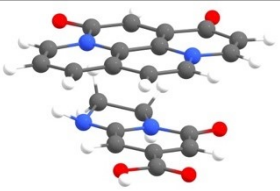# 5. Stacked complexes — O-functionalization

Two conformations differing in mutual orientation of molecular units were studied for O-functionalized stacked dimers. It was observed that the angle between the main molecular axes of IPCA and PAH only slightly affected the absorption spectra (Figure 2c–g). The O-functionalization of the PAH units with oxo-groups significantly changed the character of the CT transitions, which were primarily from PAH to IPCA in **stacked_core** and **stacked_edge** models. Moreover, the presence of oxo-groups on the edges enriched the ensemble of electronic excitations by $n \to \pi^*$ transitions.

Table S16. NTO orbitals (only those with weight > 0.10 are shown; the isocontour value is 0.04 au), vertical excitation energies (VEEs, or vertical emission energy for the first row in the table) and the calculated CT distance[21,22] displayed for electronic over 280 nm for **oxo_stacked1_a** model.

NTO (weight)	Hole	Electron	VEE (nm)	Oscillator strength	D_{CT} (Å)
S_1 Emission			501	0.558	
S_1 (0.98)			453	0.250	0.73
S_2 (0.97)			385	0.166	2.46
S_3 (0.98)			358	0.049	3.07
S_4 (0.89)			333	0.042	2.10

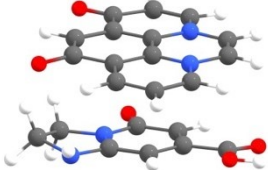| NTO (weight)	Hole	Electron	VEE (nm)	Oscillator strength	D_{CT} (Å)
S_4 (0.10)					
S_5 (0.94)			327	0.041	2.93
S_6 (0.93)			298	0.066	1.39
S_7 (0.99)			285	0.000	2.58
S_8 (0.55)			281	0.035	0.49
S_8 (0.44)					

Table S17. NTO orbitals (only those with weight > 0.10 are shown; the isocontour value is 0.04 au), vertical excitation energies (VEEs, or vertical emission energy for the first row in the table) and the calculated CT distance[21,22] displayed for electronic over 280 nm for **oxo_stacked1_b** model.

NTO (weight)	Hole	Electron	VEE (nm)	Oscillator strength	D_{CT} (Å)
S_1 Emission			525	0.464	
S_1 (0.98)			447	0.248	0.78
S_2 (0.95)			383	0.130	2.45
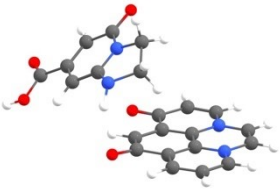
S_3 (0.97)			350	0.054	3.57
S_4 (0.97)			346	0.073	1.86
S_5 (0.99)			335	0.027	3.21
S_6 (0.94)			297	0.062	1.30
S_7 (0.99)			284	0.000	2.62
S_8 (0.66)					
S_8 (0.20)			281	0.020	3.32
S_8 (0.14)					
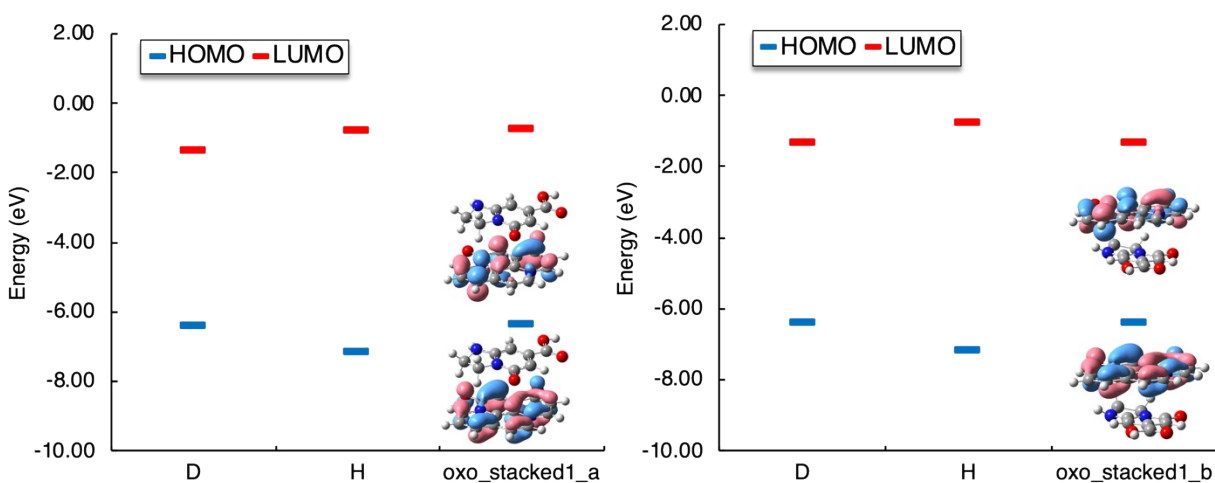
Figure S9. HOMO and LUMO orbitals of the studied systems calculated with CAM-B3LYP-D3/def2-TZVP/SMD calculations.

Table S18. NTO orbitals (only those with weight > 0.10 are shown; the isocontour value is 0.04 au), vertical excitation energies (VEEs, or vertical emission energy for the first row in the table) and the calculated CT distance[21,22] displayed for electronic over 280 nm for **oxo_stacked2_a** model.

NTO (weight)	Hole	Electron	VEE (nm)	Oscillator strength	D_{CT} (Å)
S_1 Emission*			976	0.093	
S_1 (0.99)			520	0.061	2.74
S_2 (0.95)			373	0.226	1.22
S_3 (0.98)			346	0.120	1.82
S_4 (0.51)			310	0.024	1.77
S_4 (0.48)					
S_5 (0.68)			308	0.003	2.10
S_5 (0.32)					
S_6 (0.73)			303	0.052	3.48
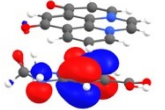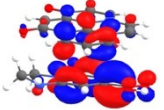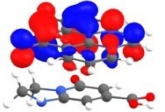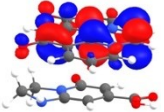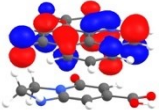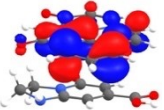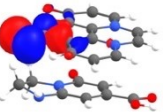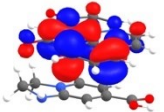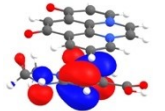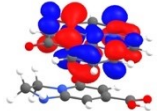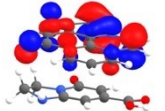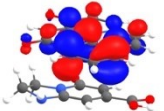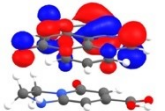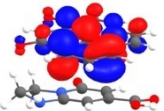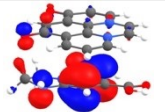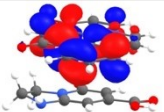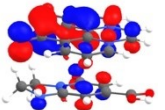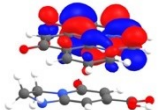
| NTO (weight)	Hole	Electron	VEE (nm)	Oscillator strength	D_{CT} (Å)
S_6 (0.25)					
S_7 (0.98)			289	0.001	3.09
S_8 (0.84)			284	0.120	2.90
S_8 (0.14)					

*Interestingly, the **oxo_stacked2_a** structure closed itself during the geometry optimization of the S_1 state preserving the character of NTO orbitals in the GS geometry (Table S17, Figure S17).

Table S19. NTO orbitals (only those with weight > 0.10 are shown; the isocontour value is 0.04 au), vertical excitation energies (VEEs, or vertical emission energy for the first row in the table) and the calculated CT distance[21,22] displayed for electronic over 280 nm for **oxo_stacked2_b** model.

NTO (weight)	Hole	Electron	VEE (nm)	Oscillator strength	D_{CT} (Å)
S_1 Emission			952	0.091	
S_1 (1.00)			529	0.050	2.73
S_2 (0.92)			378	0.161	1.36
S_3 (0.92)			352	0.075	2.73
S_4 (0.93)			348	0.020	3.82

|					
S$_5$ (0.98)			343	0.041	2.26
S$_6$ (0.83)			305	0.050	
S$_6$ (0.16)					2.43
S$_7$ (0.98)			292	0.000	3.04
S$_8$ (0.78)			287	0.031	3.21
S$_8$ (0.18)					
S$_9$ (0.63)					
S$_9$ (0.22)			286	0.082	2.43
S$_9$ (0.15)					
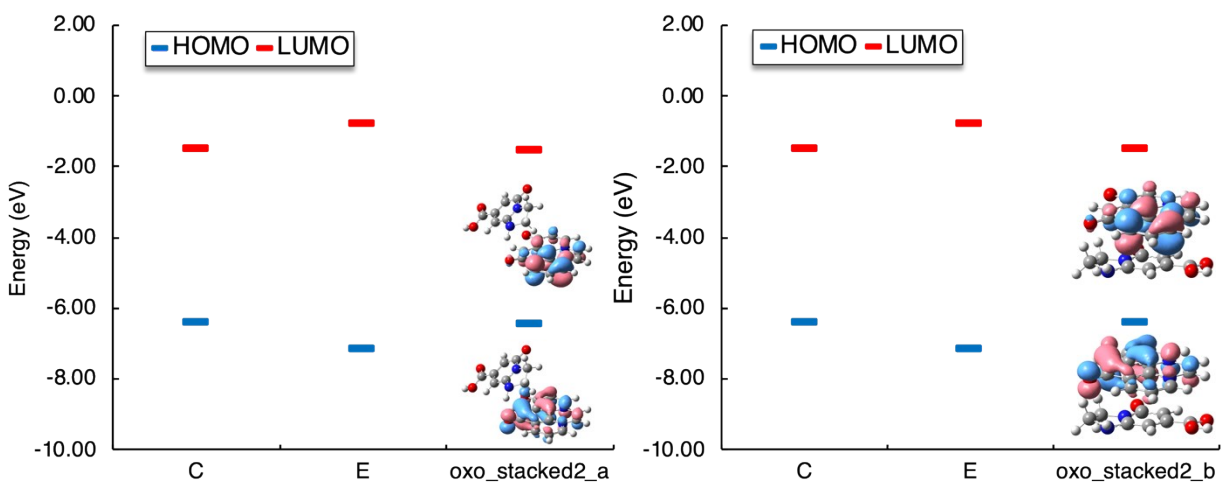
Figure S10. HOMO and LUMO orbitals of the studied systems calculated with CAM-B3LYP-D3/def2-TZVP/SMD calculations.

To sum up the findings for stacking complexes, the MO overlap of the small centres of PL brought new excitations with CT character. The facts that the nature of the structure of CDs makes such arrangements highly probable and that these CT can be sensitive to changes of the environment of CD, these states should be considered in the interpretation of the CDs PL.

The O-functionalization of the studied stacked complexes not only significantly enhanced the intensity of $S_1 \rightarrow S_0$ emission, but also made the options for more complex structural features due to possible formation of H-bonds. This could affect the overlap of the molecular units in a complex, which is essential for the enhancement of mutual communication of PL centres in CDs.
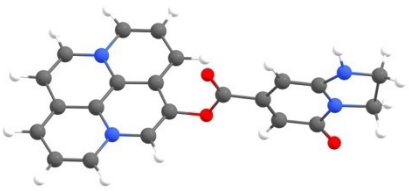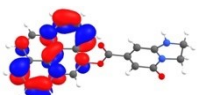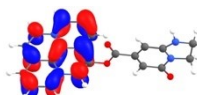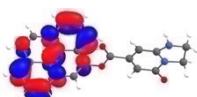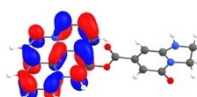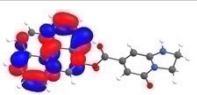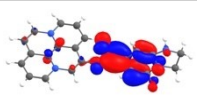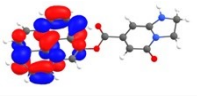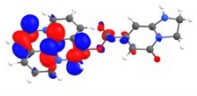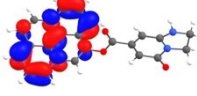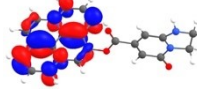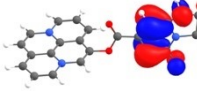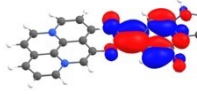
6. Single-bonded systems

To investigate the communication between core and molecular states in models separated by a single covalent bond, systems **B** and **C** were used as exemplars of the interacting PAH/IPCA units linked via ester or amide bonds. For the amide bond, three different binding PAH–IPCA positions were considered to address the geometrical and steric effects on the optical properties.
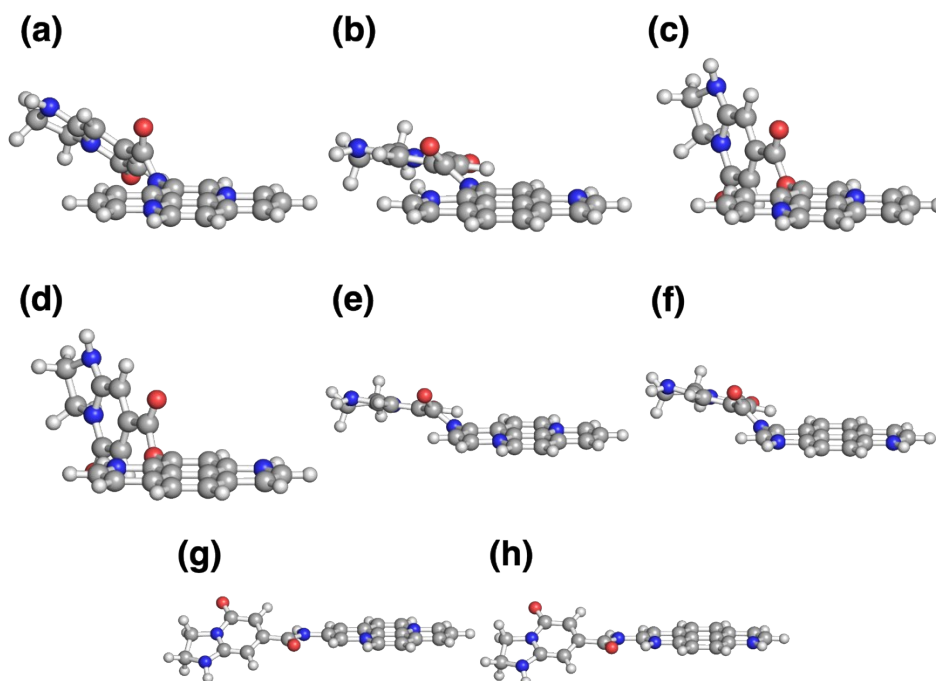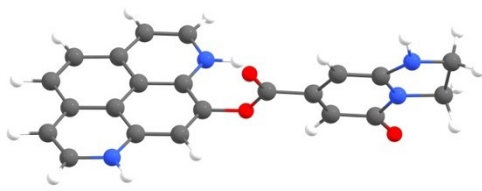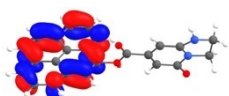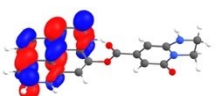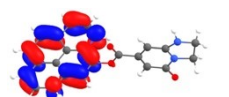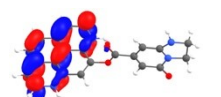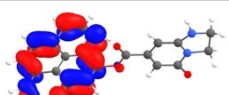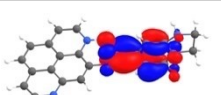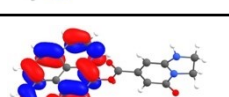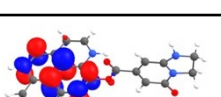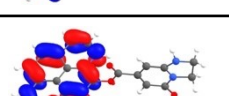

Figure S11. Side view of the single-bonded (a) amide1_core, (b) amide1_edge, (c) ester1_core, (d) ester1_edge, (e) amide2_core, (f) amide2_edge, (g) amide3_core, (h) amide3_edge complexes, displaying different mutual orientation of PAH with respect to IPCA.

Table S20. NTO orbitals (only those with weight > 0.10 are shown; the isocontour value is 0.04 au), vertical excitation energies (VEEs, or vertical emission energy for the first row in the table) and the calculated CT distance[21,22] displayed for electronic over 280 nm for **ester1_core** model.
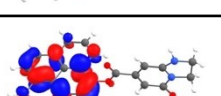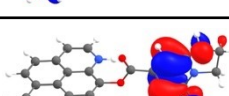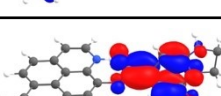
NTO (weight)	Hole	Electron	VEE (nm)	Oscillator strength	D_{CT} (Å)
S_1 Emission			1370	0.001	
S_1 (0.99)			748	0.001	0.31
S_2 (1.00)			556	0.004	5.44
S_3 (0.98)			518	0.010	0.73
S_4 (0.99)			471	0.277	0.39
S_5 (0.99)			345	0.150	1.87

Table S21. NTO orbitals (only those with weight > 0.10 are shown; the isocontour value is 0.04 au), vertical excitation energies (VEEs, or vertical emission energy for the first row in the table) and the calculated CT distance[21,22] displayed for electronic over 280 nm for **ester1_edge** model.

NTO (weight)	Hole	Electron	VEE (nm)	Oscillator strength	D_{CT} (Å)
S_1 Emission			751	0.080	
S_1 (0.99)			493	0.045	0.70
S_2 (1.00)			472	0.007	5.61
S_3 (0.97)			428	0.108	0.02
S_4 (0.98)			354	0.271	0.65
S_5 (0.99)			345	0.149	1.85
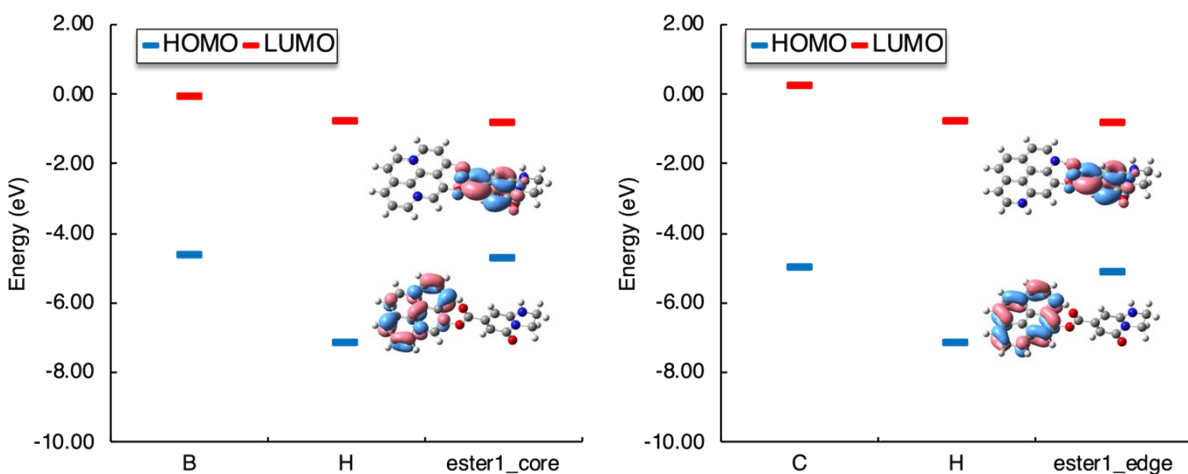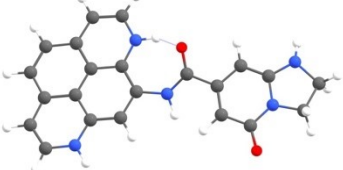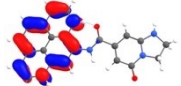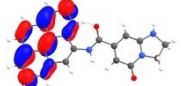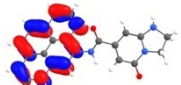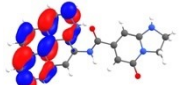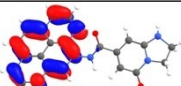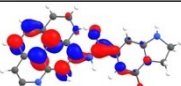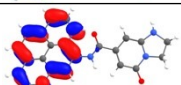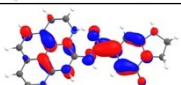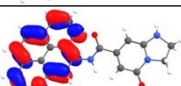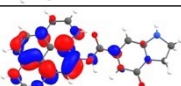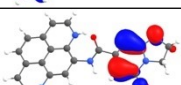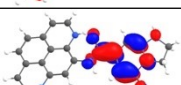
Figure S12. HOMO and LUMO orbitals of the studied systems calculated with CAM-B3LYP-D3/def2-TZVP/SMD calculations.

Table S22. NTO orbitals (only those with weight > 0.10 are shown; the isocontour value is 0.04 au), vertical excitation energies (VEEs, or vertical emission energy for the first row in the table) and the calculated CT distance[21,22] displayed for electronic over 280 nm for **amide1_core** model.

NTO (weight)	Hole	Electron	VEE (nm)	Oscillator strength	D_{CT} (Å)
S_1 Emission			1372	0.001	
S_1 (0.99)			738	0.000	0.21
S_2 (0.94)			528	0.012	0.02
S_3 (0.99)			472	0.273	0.12
S_4 (1.00)			446	0.001	6.01
S_5 (0.98)			315	0.173	1.42

Table S23. NTO orbitals (only those with weight > 0.10 are shown; the isocontour value is 0.04 au), vertical excitation energies (VEEs, or vertical emission energy for the first row in the table) and the calculated CT distance[21,22] displayed for electronic over 280 nm for **amide1_edge** model.

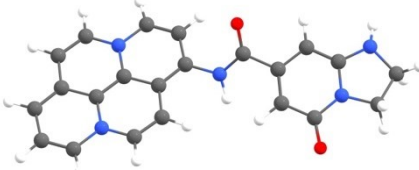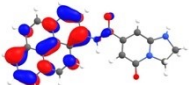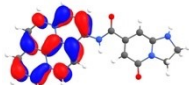| NTO (weight)	Hole	Electron	VEE (nm)	Oscillator strength	D_{CT} (Å)
S_1 Emission			757	0.081	
S_1 (0.99)			482	0.058	0.95
S_2 (0.98)			444	0.177	2.28
S_3 (0.98)			385	0.020	4.89
S_4 (0.98)			350	0.231	1.98
S_5 (0.98)			316	0.174	1.57

Table S24. NTO orbitals (only those with weight > 0.10 are shown; the isocontour value is 0.04 au), vertical excitation energies (VEEs, or vertical emission energy for the first row in the table) and the calculated CT distance[21,22] displayed for electronic over 280 nm for **amide2_core** model.

NTO (weight)	Hole	Electron	VEE (nm)	Oscillator strength	D_{CT} (Å)
S_1 Emission			1464	0.009	
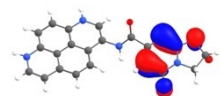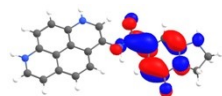
NTO (weight)	Hole	Electron	VEE (nm)	Oscillator strength	D_CT (Å)
S_1 (0.99)			749	0.003	0.15
S_2 (0.98)			528	0.013	0.08
S_3 (0.99)			497	0.363	2.21
S_4 (0.99)			425	0.065	6.02
S_5 (0.98)			313	0.180	1.51
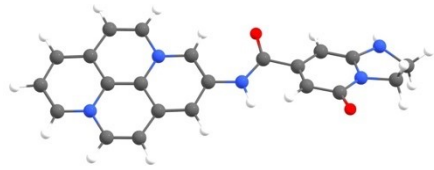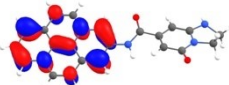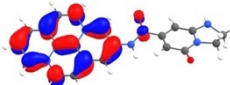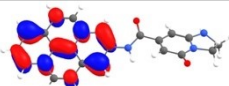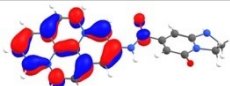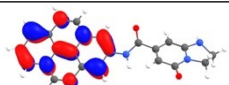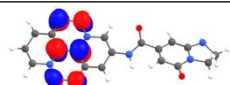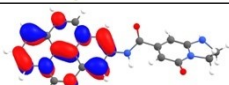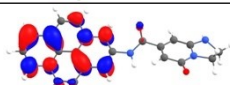
Table S25. NTO orbitals (only those with weight > 0.10 are shown; the isocontour value is 0.04 au), vertical excitation energies (VEEs, or vertical emission energy for the first row in the table) and the calculated CT distance[21,22] displayed for electronic over 280 nm for **amide2_edge** model.

NTO (weight)	Hole	Electron	VEE (nm)	Oscillator strength	D_{CT} (Å)
S_1 Emission			782	0.051	
S_1 (0.99)			505	0.035	0.98
S_2 (0.97)			430	0.058	0.35
S_3 (0.99)			391	0.172	5.95
S_4 (0.98)			351	0.222	1.31
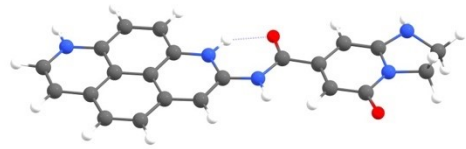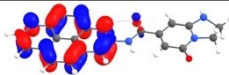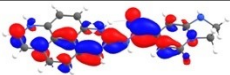
S$_5$ (0.98)			312	0.189	1.38

Table S26. NTO orbitals (only those with weight > 0.10 are shown; the isocontour value is 0.04 au), vertical excitation energies (VEEs, or vertical emission energy for the first row in the table) displayed for electronic over 280 nm for **amide3_core** model.

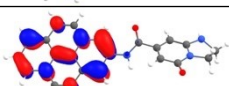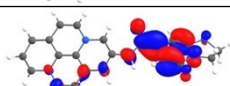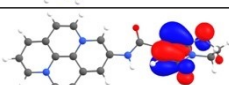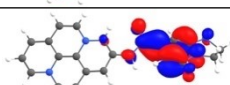| NTO (weight)	Hole	Electron	VEE (nm)	Oscillator strength	D$_{CT}$ (Å)
S$_1$ Emission			1310	0.004	
S$_1$ (0.99)			754	0.007	0.89
S$_2$ (0.98)			529	0.015	0.06
S$_3$ (0.99)			485	0.260	0.18
S$_4$ (1.00)			430	0.279	6.57
S$_5$ (0.98)			319	0.163	1.82

Table S27. NTO orbitals (only those with weight > 0.10 are shown; the isocontour value is 0.04 au), vertical excitation energies (VEEs, or vertical emission energy for the first row in the table) and the calculated CT distance[21,22] displayed for electronic over 280 nm for **amide3_edge** model.

NTO (weight)	Hole	Electron	VEE (nm)	Oscillator strength	D$_{CT}$ (Å)
S$_1$ Emission			1400	0.181	
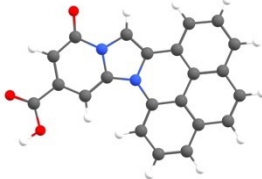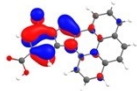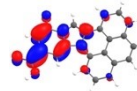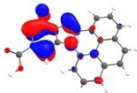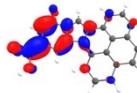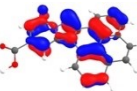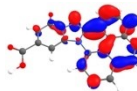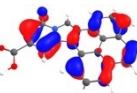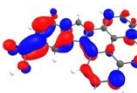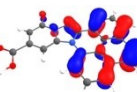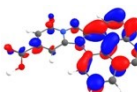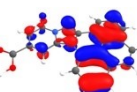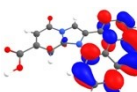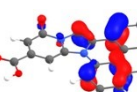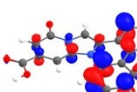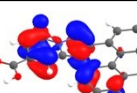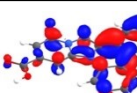
S_1 (0.98)			539	0.122	2.78
S_2 (0.97)			434	0.060	0.11
S_3 (0.99)			378	0.038	5.68
S_4 (0.98)			362	0.348	0.87
S_5 (0.99)			325	0.153	1.96
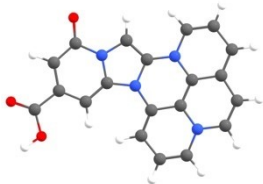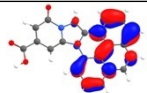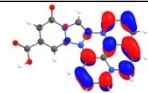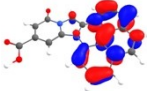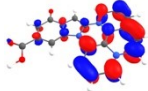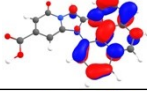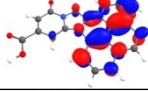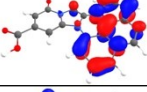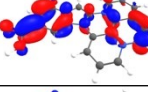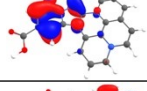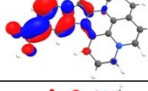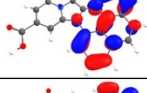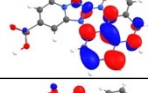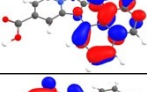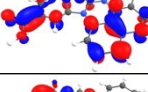
Figure S13. HOMO and LUMO orbitals of the studied systems calculated with CAM-B3LYP-D3/def2-TZVP/SMD calculations.
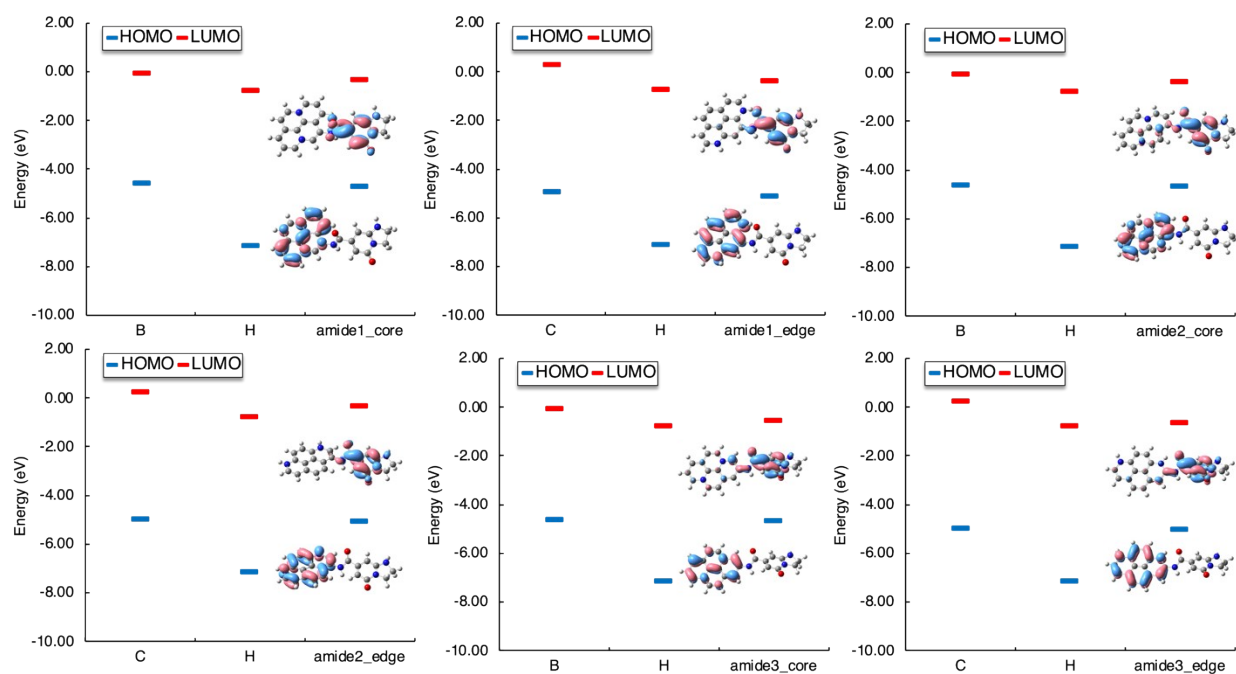
7. Fused systems

Table S28. NTO orbitals (only those with weight > 0.10 are shown; the isocontour value is 0.04 au), vertical excitation energies (VEEs, or vertical emission energy for the first row in the table) and the calculated CT distance[21,22] displayed for electronic over 280 nm for **fused** model.

NTO (weight)	Hole	Electron	VEE (nm)	Oscillator strength	D_{CT} (Å)
S_1 Emission			441	0.834	
S_1 (0.97)			379	0.557	1.50
S_2 (0.68)			315	0.014	2.11
S_2 (0.24)					
S_3 (0.58)			304	0.073	0.50
S_3 (0.38)					
S_4 (0.60)			281	0.439	1.05
S_4 (0.38)					

Table S29. NTO orbitals (only those with weight > 0.10 are shown; the isocontour value is 0.04 au), vertical excitation energies (VEEs, or vertical emission energy for the first row in the table) and the calculated CT distance[21,22] displayed for electronic over 280 nm for **fused_core** model.

NTO (weight)	Hole	Electron	VEE (nm)	Oscillator strength	D_{CT} (Å)
S_1 Emission			1071	0.005	
S_1 (0.99)			651	0.003	1.46
S_2 (0.99)			512	0.217	0.98
S_3 (0.99)			503	0.079	4.16
S_4 (0.84)			363	0.392	
S_4 (0.14)					2.14
S_5 (0.86)			354	0.026	
S_5 (0.12)					3.53
S_6 (0.95)			283	0.242	4.57

Table S30. NTO orbitals (only those with weight > 0.10 are shown; the isocontour value is 0.04 au), vertical excitation energies (VEEs, or vertical emission energy for the first row in the table) and the calculated CT distance[21,22] displayed for electronic over 280 nm for the **fused_edge** model.

NTO (weight)	Hole	Electron	VEE (nm)	Oscillator strength	D_{CT} (Å)
S_1 Emission			945	0.023	
S_1 (0.99)			592	0.122	1.13
S_2 (0.98)			558	0.453	4.55
S_3 (0.99)			512	0.198	1.73
S_4 (0.82)			350	0.016	2.30
S_4 (0.15)					
S_5 (0.83)			338	0.113	2.70
S_5 (0.15)					
S_6 (0.74)			303	0.032	0.93
S_6 (0.24)					

S_7 (0.73)			283	0.014	3.11
S_7 (0.27)					

Figure S14. HOMO and LUMO orbitals of the studied systems calculated with CAM-B3LYP-D3/def2-TZVP/SMD calculations.

8. Calculations with systems containing bigger core (N-doped coronene moiety)
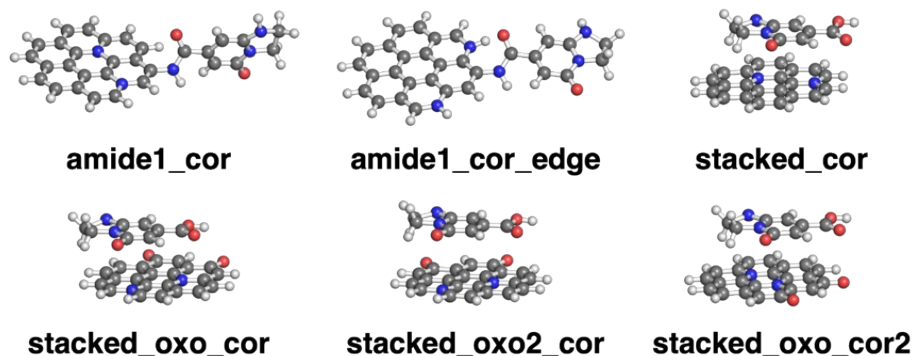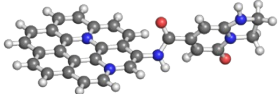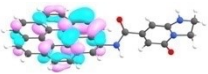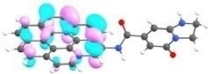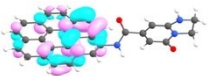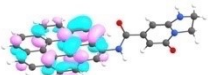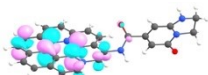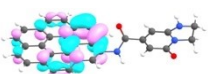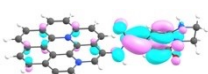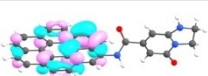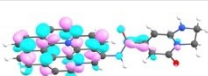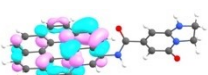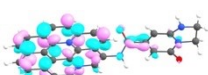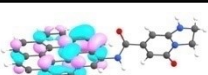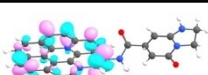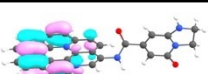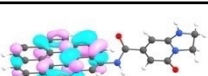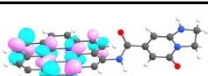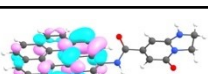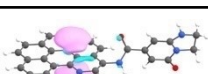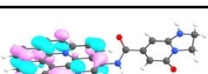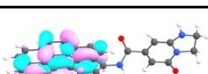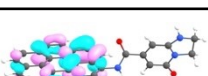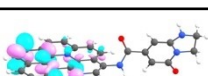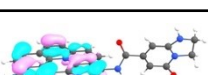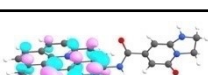
Figure S15. Studied interaction motifs of PAH/IPCA, where the CD core is represented by an N-doped coronene-sized PAH.
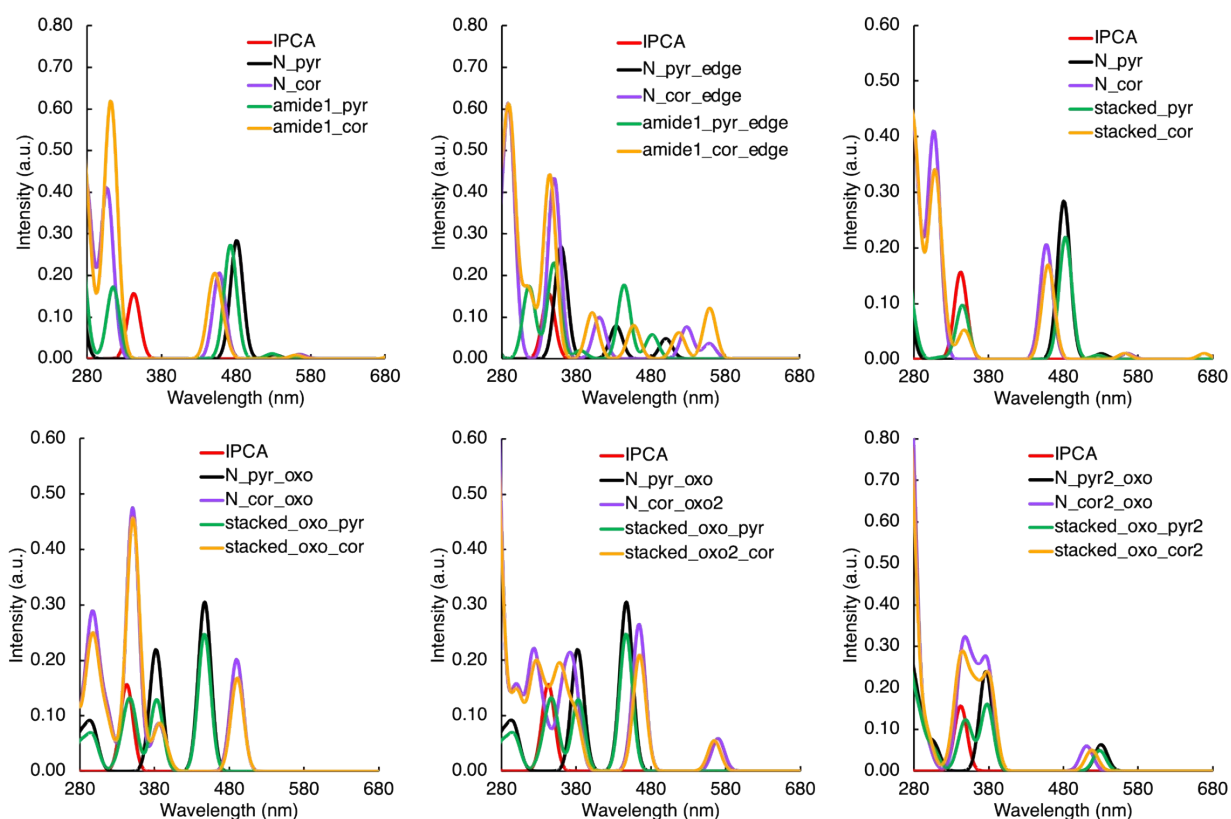
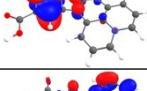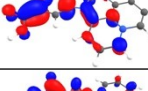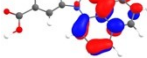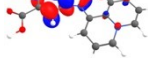**Figure S16.** Absorption spectra of coronene/IPCA and pyrene/IPCA complexes along with those of the separated molecules which form the complexes. For each spectrum, the line spectra (excitation energy of 30 lowest singlet states with different oscillator strengths) were convoluted by a Gaussian function assuming the inhomogeneous broadening of peaks with σ = 20 nm, and the absorption range from 280 to 680 nm is shown.
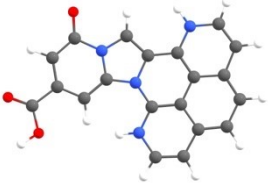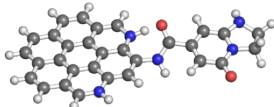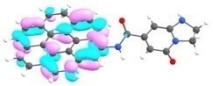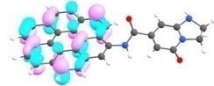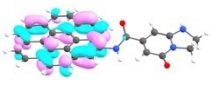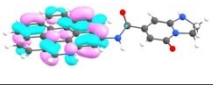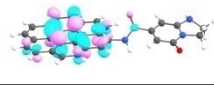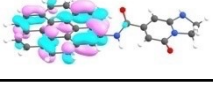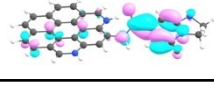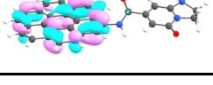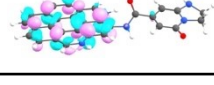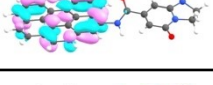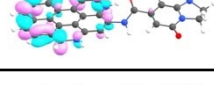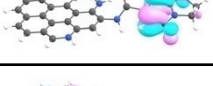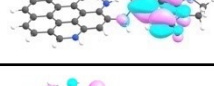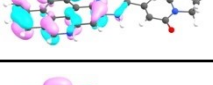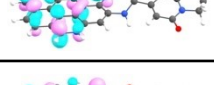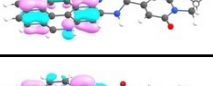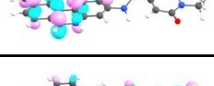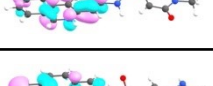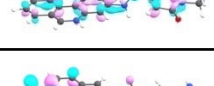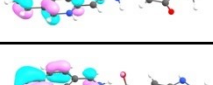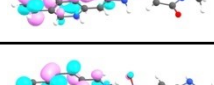
Table S31. NTO orbitals (only those with weight > 0.10 are shown; the isocontour value is 0.04 au), vertical excitation energies (VEEs) and the calculated CT distance displayed for ten lowest excited states for the **amide1_cor** model.

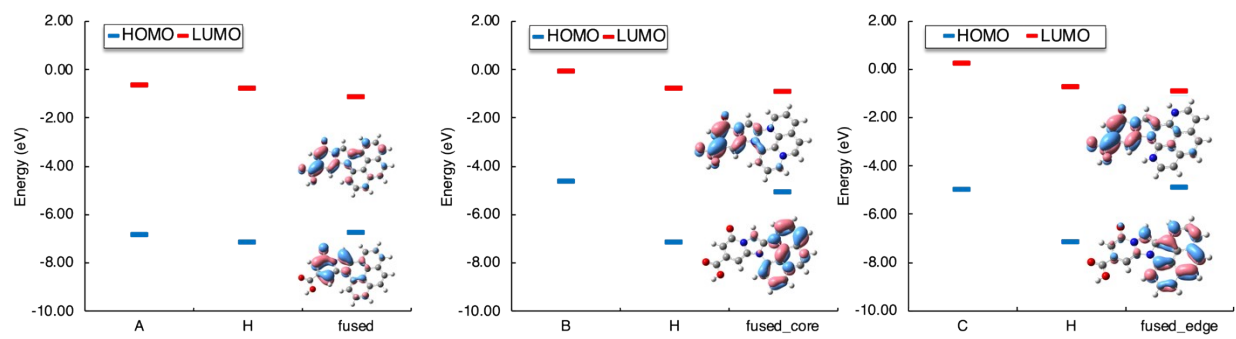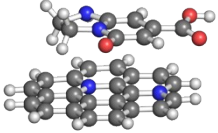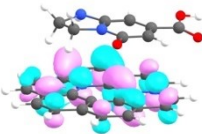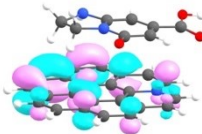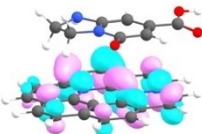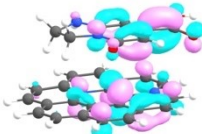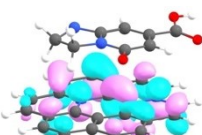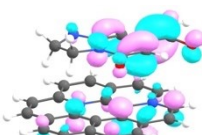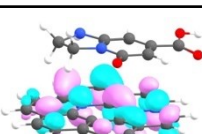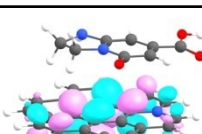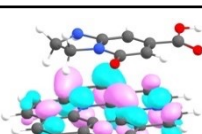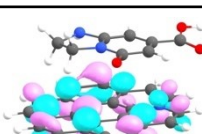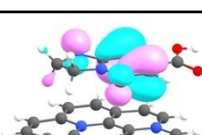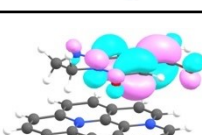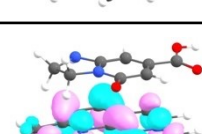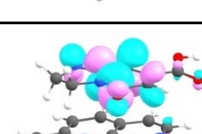| NTO (weight)	Hole	Electron	VEE (nm)	Oscillator strength	D_{CT} (Å)
S_1 (0.99)			909	0.006	0.99
S_2 (0.99)			695	0.020	2.17
S_3 (0.98)			560	0.009	0.89
S_4 (0.99)			460	0.068	5.40
S_5 (0.98)			449	0.172	0.36
S_6 (0.98)			316	0.208	1.49
S_7 (0.90)			310	0.413	0.15
S_8 (0.51)			301	0.056	1.44
S_8 (0.42)					
S_9 (0.97)			282	0.005	0.69
S_{10} (0.68)			277	0.340	1.09
S_{10} (0.20)					
S_{10} (0.10)					

Table S32. NTO orbitals (only those with weight > 0.10 are shown; the isocontour value is 0.04 au), vertical excitation energies (VEEs) and the calculated CT distance displayed for ten lowest excited states for the **amide1_cor_edge** model.

NTO (weight)	Hole	Electron	VEE (nm)	Oscillator strength	D_{CT} (Å)
S_1 (0.99)			897	0.077	1.72
S_2 (0.98)			559	0.122	1.04
S_3 (0.98)			517	0.063	0.26
S_4 (0.99)			457	0.080	5.50
S_5 (0.98)			401	0.111	0.19
S_6 (0.94)			344	0.443	1.96
S_7 (0.98)			315	0.164	1.58
S_8 (0.95)			292	0.258	1.24
S_9 (0.95)			288	0.331	1.22
S_{10} (0.72)					
S_{10} (0.14)			273	0.224	4.07
S_{10} (0.11)					
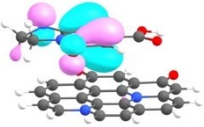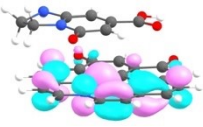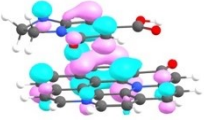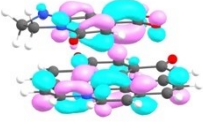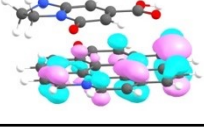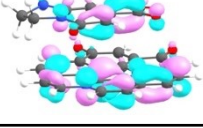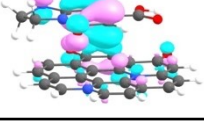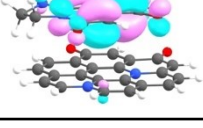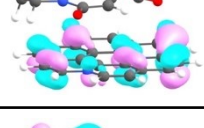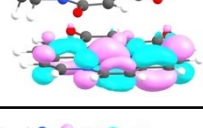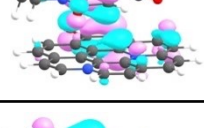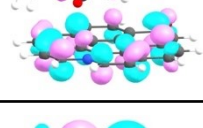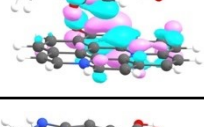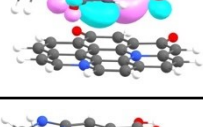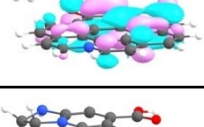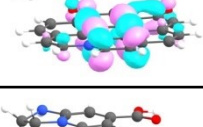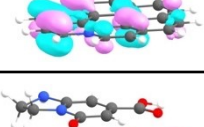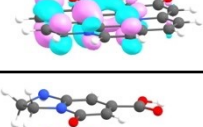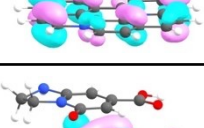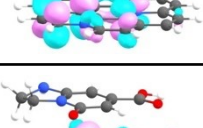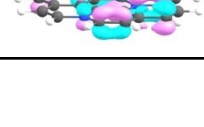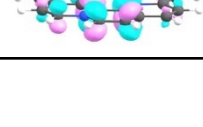
Table S33. NTO orbitals (only those with weight > 0.10 are shown; the isocontour value is 0.04 au), vertical excitation energies (VEEs) and the calculated CT distance displayed for ten lowest excited states for the **stacked_cor** model.

NTO (weight)	Hole	Electron	VEE (nm)	Oscillator strength	D_{CT} (Å)
S_1 (0.99)			938	0.006	1.12
S_2 (0.99)			732	0.011	2.73
S_3 (0.99)			669	0.010	3.07
S_4 (0.98)			562	0.011	1.13
S_5 (0.99)			460	0.170	1.54
S_6 (0.97)			347	0.052	1.85
S_7 (0.98)			320	0.030	3.27

	Hole	Electron	VEE (nm)	Oscillator strength	D_{CT} (Å)
S_8 (0.88)			309	0.261	0.80
S_9 (0.48)			304	0.076	1.55
S_9 (0.45)					
S_{10} (0.98)			287	0.004	1.12

Table S34. NTO orbitals (only those with weight > 0.10 are shown; the isocontour value is 0.04 au), vertical excitation energies (VEEs) and the calculated CT distance displayed for ten lowest excited states for the **stacked_oxo_cor** model.

NTO (weight)	Hole	Electron	VEE (nm)	Oscillator strength	D_{CT} (Å)
S_1 (0.97)			491	0.169	3.74
S_2 (0.61)			394	0.015	3.09
S2 (0.38)					
S_3 (0.94)			386	0.076	3.04
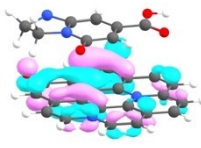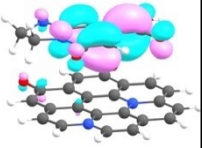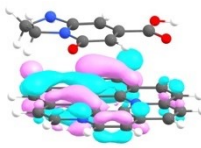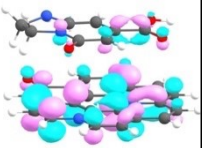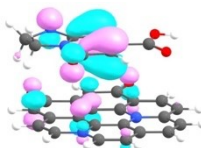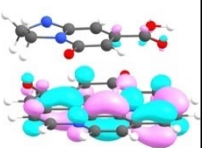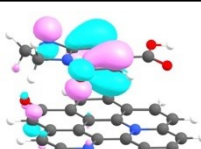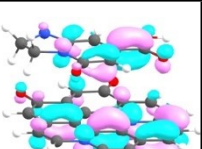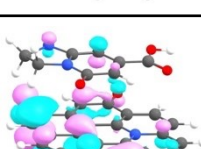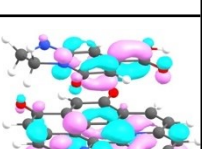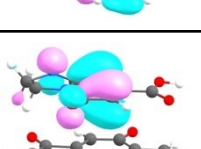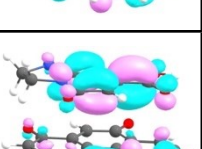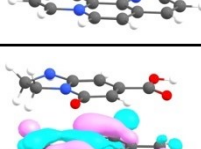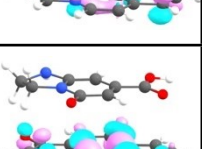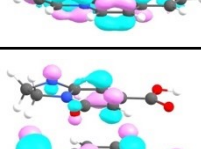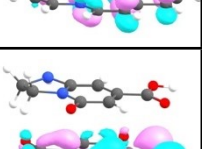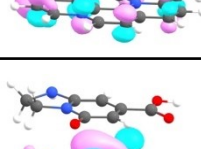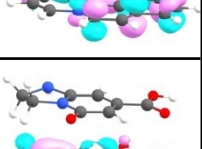
S$_4$ (0.97)			365	0.022	3.50
S$_5$ (0.59)			352	0.241	2.88
S$_5$ (0.31)					
S$_6$ (0.68)			351	0.191	2.28
S$_6$ (0.21)					
S$_6$ (0.10)					
S$_7$ (0.98)			341	0.044	3.72
S$_8$ (0.78)			316	0.085	3.31
S$_8$ (0.15)					
S$_9$ (0.71)			301	0.068	2.42
S$_9$ (0.18)					
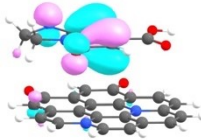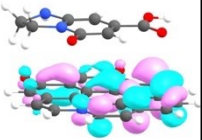
NTO (weight)	Hole	Electron	VEE (nm)	Oscillator strength	D_{CT} (Å)
S_{10} (0.60)					
S_{10} (0.26)			297	0.118	1.75
S_{10} (0.12)					

Table S35. NTO orbitals (only those with weight > 0.10 are shown; the isocontour value is 0.04 au), vertical excitation energies (VEEs) and the calculated CT distance displayed for ten lowest excited states for the **stacked_oxo2_cor** model.
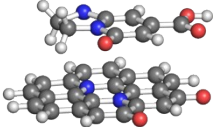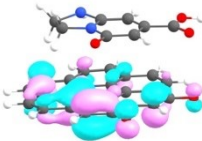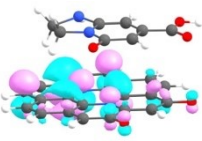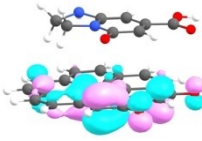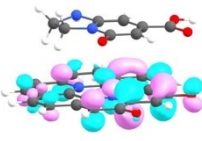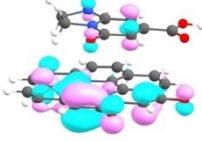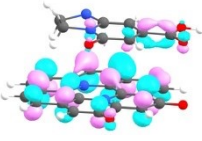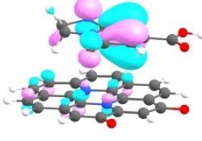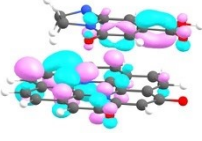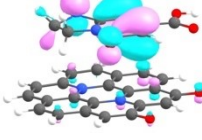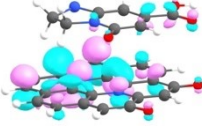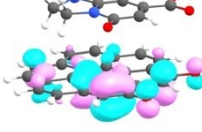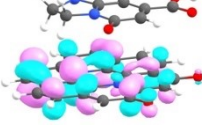
NTO (weight)	Hole	Electron	VEE (nm)	Oscillator strength	D_{CT} (Å)
S_1 (0.98)			565	0.055	2.98
S_2 (0.96)			465	0.210	3.02
S_3 (0.80)			379	0.087	3.00
S_3 (0.16)					
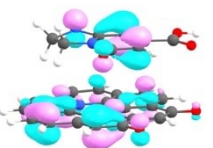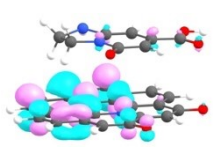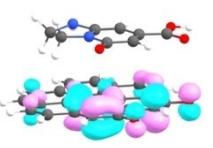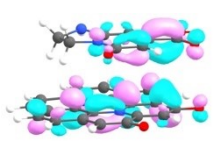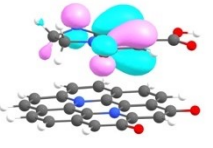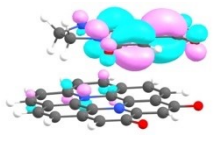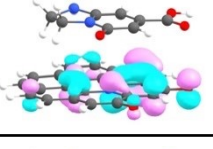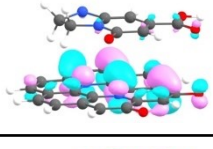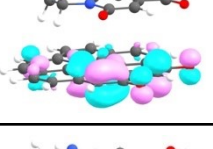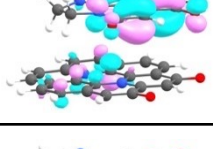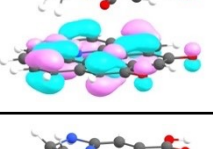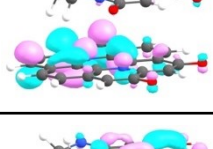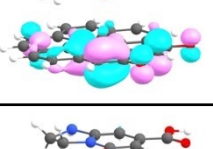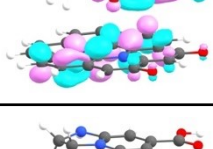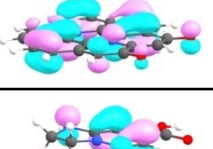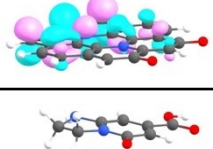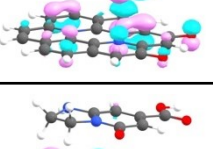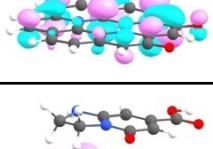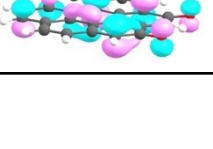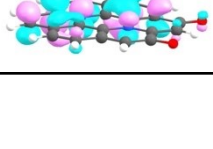
S_4 (0.98)			371	0.016	3.52
S_5 (0.72)			362	0.084	2.85
S_5 (0.26)					
S_6 (0.84)			355	0.105	3.18
S_6 (0.12)					
S_7 (0.90)			344	0.035	2.76
S_8 (0.82)			337	0.073	2.85
S_9 (0.85)			325	0.163	3.09
S_9 (0.13)					
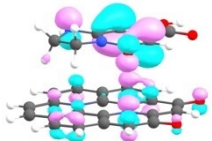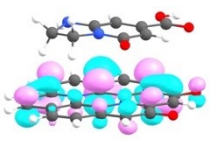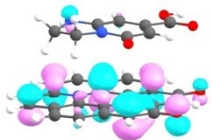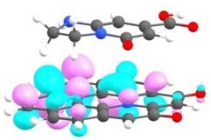
NTO (weight)	Hole	Electron	VEE (nm)	Oscillator strength	D_{CT} (Å)
S_{10} (0.94)			312	0.025	3.99

Table S36. NTO orbitals (only those with weight > 0.10 are shown; the isocontour value is 0.04 au), vertical excitation energies (VEEs) and the calculated CT distance displayed for ten lowest excited states for the **stacked_oxo_cor2** model.

NTO (weight)	Hole	Electron	VEE (nm)	Oscillator strength	D_{CT} (Å)
S_1 (0.98)			518	0.051	3.35
S_2 (0.93)			381	0.205	2.64
S_3 (0.70)			368	0.064	2.82
S_3 (0.27)					
S_4 (0.72)			361	0.109	3.39
S_4 (0.24)					

S_5 (0.56)					
			352	0.078	2.32
S_5 (0.38)					
S_6 (0.79)					
			342	0.216	1.07
S_6 (0.13)					
S_7 (0.76)					
			334	0.027	3.41
S_7 (0.23)					
S_8 (0.87)					
			320	0.003	2.64
S_8 (0.12)					
S_9 (0.86)					
			298	0.055	2.78
S_9 (0.10)					

			294	0.036	3.06
S_{10} (0.84)					
S_{10} (0.13)					

9. Differences Between Ground and Excited State Geometries

(0.130)

(0.080)   (0.091)

COOH_core   COOH_edge   stacked_core

(0.534)   (0.079)   (1.701)

stacked_edge   oxo_stacked1_a   oxo_stacked2_a

(0.551)   (0.135)

oxo_stacked1_b   oxo_stacked2_b
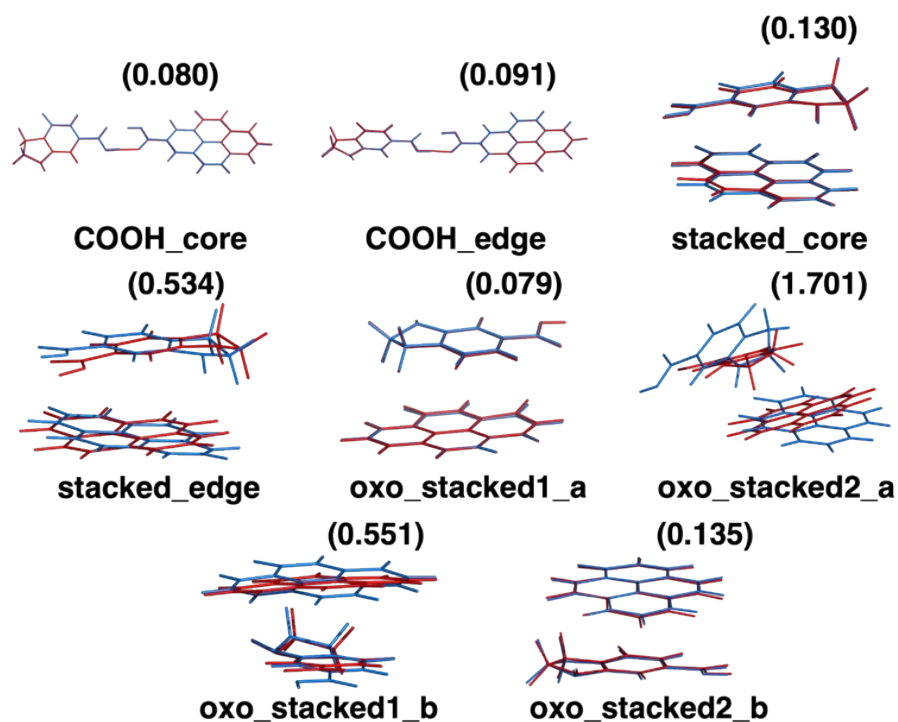
Figure S17. The difference between S_0 (blue) and S_1 (red) relaxed geometries of the studied non-bonded complexes structures (RMS is shown in brackets in Å).

(0.039)   (0.249)   (0.246)

ester1_core   ester1_edge   amide1_core

(0.266)   (0.469)   (0.495)

amide1_edge   amide2_core   amide2_edge

(0.142)   (0.549)

amide3_core   amide3_edge
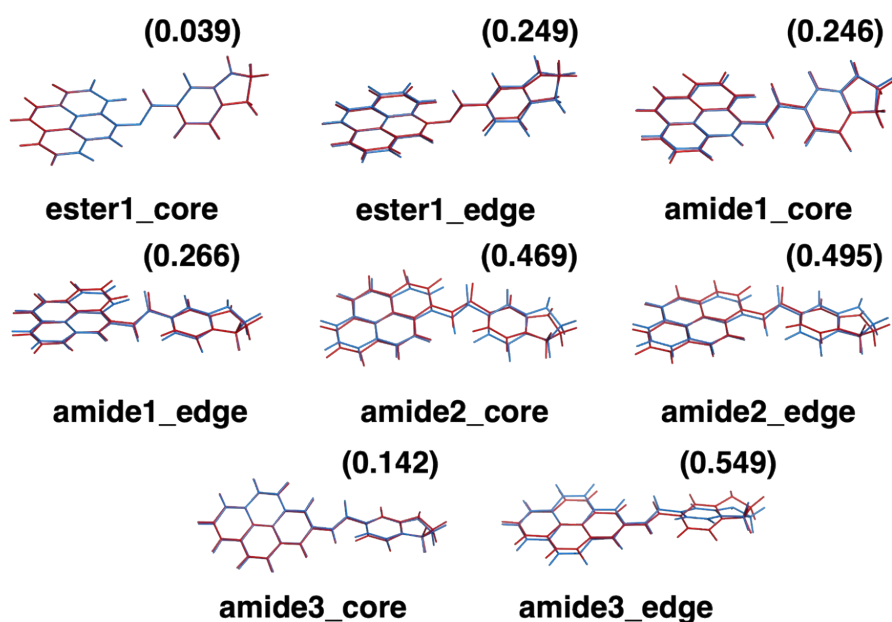
Figure S18. The difference between S_0 (blue) and S_1 (red) relaxed geometries of the studied bonded complexes (RMS is shown in brackets in Å).
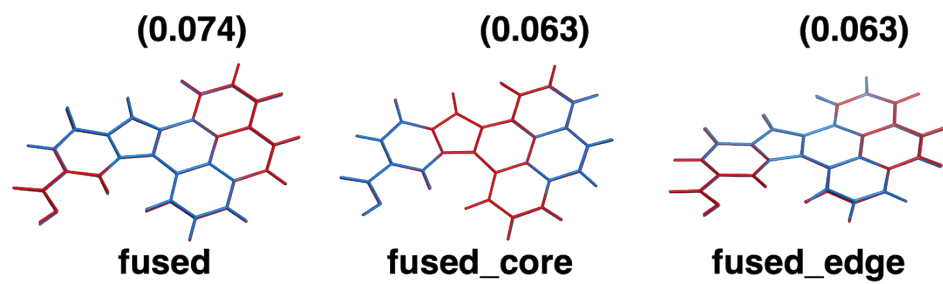
Figure S19. The difference between S_0 (blue) and S_1 (red) relaxed geometries of the studied fused complexes (RMS is shown in brackets in Å).

10. Excitation energy transfer analysis

Table S37. Calculated values of electronic coupling for excitation energy transfer between the molecular units of the complex **COOH_core**. The values in the matrix are total coupling (in eV). The value in the violet frame corresponds the ET displayed in the de-excitation cascade scheme (Figure 4a). The letters in the grey cell refer to the molecular systems (see Figure S1) forming the studied complex.

VEE (nm) →		341	242	232	223	213
↓	↓F/H→	S_1	S_2	S_3	S_4	S_5
832	S_1	0.00034	-0.00091	0.00019	-0.00093	-0.00678
489	S_2	0.00013	-0.00035	0.00007	-0.00030	-0.00279
461	S_3	0.00091	0.00069	-0.00009	0.00024	0.00606
342	S_4	0.00191	-0.00216	0.00041	-0.00178	-0.01769
262	S_5	-0.00073	-0.00175	0.00028	-0.00121	-0.01409

$S_6 \rightarrow S_5$ in dimer

Table S38. Calculated values of electronic coupling for excitation energy transfer between the molecular units of the complex **COOH_edge**. The values in the matrix are total coupling (in eV). The value in the violet frame corresponds the ET displayed in the de-excitation cascade scheme (Figure 4b). The letters in the grey cell refer to the molecular systems (see Figure S1) forming the studied complex.

VEE (nm) →		342	242	233	223	213
↓	↓G/H→	S_1	S_2	S_3	S_4	S_5
649	S_1	-0.00018	-0.00085	-0.00121	0.00128	-0.01033
428	S_2	-0.00152	0.00005	0.00007	-0.00007	0.00074
356	S_3	-0.00017	0.00056	0.00069	-0.00042	0.00763
312	S_4	0.00187	0.00065	0.00099	-0.00123	0.00722
253	S_5	0.00160	0.00032	0.00053	-0.00075	0.00308

$S_5 \rightarrow S_4$ in dimer

Table S39. Calculated values of electronic coupling for excitation energy transfer between the molecular units of the complex **stacked_core**. The values in the matrix are total coupling (in eV). The value in the violet frame corresponds the ET displayed in the de-excitation cascade scheme (Figure 4c). The letters in the grey cell refer to the molecular systems (see Figure S1) forming the studied complex.

VEE (nm)	→	340	240	231	223	214
↓	↓B/H→	S_1	S_2	S_3	S_4	S_5
752	S_1	-0.00152	-0.00037	0.00098	-0.00655	-0.00558
531	S_2	-0.00988	-0.00002	0.00297	-0.00047	0.01527
480	S_3	-0.05925	-0.00302	0.00707	0.00497	0.03912
272	S_4	-0.00784	0.00183	0.00114	-0.00700	-0.00341
265	S_5	0.02038	-0.00498	0.00164	0.00601	0.04605

$S_5 \rightarrow S_4$ in dimer

Table S40. Calculated values of electronic coupling for excitation energy transfer between the molecular units of the complex **stacked_edge**. The values in the matrix are total coupling (in eV). The value in the violet frame corresponds the ET displayed in the de-excitation cascade scheme (Figure 4d). The letters in the grey cell refer to the molecular systems (see Figure S1) forming the studied complex.

VEE (nm)	→	342	240	232	224	214
↓	↓C/H→	S_1	S_2	S_3	S_4	S_5
499	S_1	-0.02544	-0.00082	-0.00157	0.00302	-0.01003
431	S_2	-0.00843	0.00111	0.00278	-0.00056	0.03581
359	S_3	0.05661	0.00076	0.00483	-0.00608	0.02544
258	S_4	-0.01616	0.00409	0.00130	-0.00730	0.04713
248	S_5	0.00746	-0.00069	0.00040	0.00048	0.00069

$S_5 \rightarrow S_4$ in dimer $S_4 \rightarrow S_3$ in dimer

Table S41. Calculated values of electronic coupling for excitation energy transfer between the molecular units of the complex **oxo_stacked1_a**. The values in the matrix are total coupling (in eV). The value in the violet frame corresponds the ET displayed in the de-excitation cascade scheme (Figure 4e). The letters in the grey cell refer to the molecular systems (see Figure S1) forming the studied complex.

VEE (nm)	→	343	240	231	224	213
↓	↓D/H→	S_1	S_2	S_3	S_4	S_5
446	S_1	0.02356	0.00121	0.00234	-0.00944	0.05072
382	S_2	0.02960	-0.00140	-0.00393	0.00097	-0.03824
296	S_3	-0.02702	-0.00264	0.00010	-0.00178	-0.00640
285	S_4	0.00109	-0.00007	-0.00025	0.00094	-0.00321
279	S_5	-0.01611	0.00362	0.00236	-0.00138	0.02516

$S_5 \rightarrow S_4$ in dimer

Table S42. Calculated values of electronic coupling for excitation energy transfer between the molecular units of the complex **oxo_stacked1_b**. The values in the matrix are total coupling (in eV). The letters in the grey cell refer to the molecular systems (see Figure S1) forming the studied complex.

VEE (nm)	→	342	240	231	224	214
↓	↓D/H→	S_1	S_2	S_3	S_4	S_5
446	S_1	-0.01881	-0.00114	-0.00042	0.00465	-0.06291
382	S_2	0.04745	-0.00070	-0.00259	0.00043	-0.00247
296	S_3	-0.01064	0.00011	0.00083	-0.00916	0.03053
284	S_4	0.00022	0.00008	-0.00031	-0.00211	-0.00080
279	S_5	-0.02530	-0.00040	-0.00048	-0.00463	0.00558

Table S43. Calculated values of electronic coupling for excitation energy transfer between the molecular units of the complex **oxo_stacked_2_a**. The values in the matrix are total coupling (in eV). The letters in the grey cell refer to the molecular systems (see Figure S1) forming the studied complex.

VEE (nm)	→	339	240	232	222	214
↓	↓D/H→	1	2	3	4	5
535	1	0.02302	-0.00006	0.00049	0.00425	0.00299
378	2	0.00646	-0.00097	-0.00001	0.01642	0.01995
307	3	0.00698	0.00054	-0.00227	-0.00508	0.00340
296	4	0.00009	0.00005	-0.00012	-0.00028	0.00035
287	5	0.00783	0.00022	-0.00101	-0.00001	0.00389

Table S44. Calculated values of electronic coupling for excitation energy transfer between the molecular units of the complex **oxo_stacked_2_b**. The values in the matrix are total coupling (in eV). The value in the violet frame corresponds the ET displayed in the de-excitation cascade scheme (Figure 4h). The letters in the grey cell refer to the molecular systems (see Figure S1) forming the studied complex.

VEE (nm)	→	342	239	231	224	214
↓	↓E/H→	S_1	S_2	S_3	S_4	S_5
533	S_1	0.02475	-0.00024	-0.00100	0.00535	-0.03178
376	S_2	0.02841	-0.00012	0.00065	-0.00391	0.04839
307	S_3	-0.00021	-0.00051	-0.00115	-0.01005	0.02327
295	S_4	0.00008	-0.00009	0.00004	0.00029	-0.00122
286	S_5	-0.02350	-0.00029	0.00342	0.00677	-0.00399

$S_3 \rightarrow S_2$ in dimer

Table S45. Calculated values of electronic coupling for excitation energy transfer between the molecular units of the complex **ester1_core**. The values in the matrix are total coupling (in eV). The value in the violet frame corresponds the ET displayed in the de-excitation cascade scheme (Figure 5a). The letters in the grey cell refer to the molecular systems (see Figure S1) forming the studied complex.

VEE (nm) →	↓B/H→	347 S_1	245 S_2	227 S_3	222 S_4	214 S_5
746	S_1	-0.00037	-0.00012	-0.00032	-0.00010	-0.00077
528	S_2	-0.00044	-0.00028	-0.00281	-0.00002	0.00739
478	S_3	0.00231	0.00115	0.00226	0.00006	0.00139
271	S_4	-0.00129	-0.00063	-0.00114	0.00042	0.00090
265	S_5	-0.00335	0.00003	0.00326	-0.00039	-0.01863

$S_5 \rightarrow S_4$ in dimer

Table S46. Calculated values of electronic coupling for excitation energy transfer between the molecular units of the complex **ester1_edge**. The values in the matrix are total coupling (in eV). The value in the violet frame corresponds the ET displayed in the de-excitation cascade scheme (Figure 5b). The letters in the grey cell refer to the molecular systems (see Figure S1) forming the studied complex.

VEE (nm) →	↓C/H→	316 S_1	240 S_2	218 S_3	217 S_4	209 S_5
488	S_1	-0.00131	-0.00022	-0.00003	-0.00021	-0.00413
427	S_2	-0.00150	-0.00111	0.00337	0.00187	-0.01820
358	S_3	0.00279	0.00095	0.00128	0.00023	0.00480
256	S_4	0.00301	0.00082	-0.00155	-0.00070	0.01621
249	S_5	0.00086	-0.00044	0.00060	0.00074	-0.00017

$S_5 \rightarrow S_4$ in dimer

Table S47. Calculated values of electronic coupling for excitation energy transfer between the molecular units of the complex **amide1_core**. The values in the matrix are total coupling (in eV). The letters in the grey cell refer to the molecular systems (see Figure S1) forming the studied complex.

VEE (nm) →	↓B/H→	316 S_1	239 S_2	217 S_3	217 S_4	209 S_5
742	S_1	0.00048	0.00015	-0.00009	-0.00070	-0.00047
530	S_2	0.00269	-0.00008	0.00160	0.00297	0.00859
478	S_3	-0.00818	-0.00304	0.00084	0.00398	0.00011
270	S_4	0.00091	0.00003	0.00026	-0.00002	-0.00031
265	S_5	-0.00439	0.00322	-0.00369	-0.01178	-0.01799

Table S48. Calculated values of electronic coupling for excitation energy transfer between the molecular units of the complex **amide1_edge**. The values in the matrix are total coupling (in eV). The letters in the grey cell refer to the molecular systems (see Figure S1) forming the studied complex.

VEE (nm) →		316	240	218	217	209
↓	↓C/H→	S_1	S_2	S_3	S_4	S_5
488	S_1	0.00424	0.00328	0.00163	-0.00415	-0.00444
427	S_2	-0.00718	0.00320	0.00531	-0.01042	-0.01613
358	S_3	-0.00523	-0.00776	-0.00347	0.00779	0.00743
256	S_4	0.00377	-0.00639	-0.00503	0.01085	0.01390
249	S_5	-0.00012	-0.00213	-0.00173	-0.00080	-0.00049

Table S49. Calculated values of electronic coupling for excitation energy transfer between the molecular units of the complex **amide2_core**. The values in the matrix are total coupling (in eV). The letters in the grey cell refer to the molecular systems (see Figure S1) forming the studied complex.

VEE (nm) →		315	239	217	217	209
↓	↓B/H→	S_1	S_2	S_3	S_4	S_5
750	S_1	-0.00013	-0.00160	0.00126	-0.00209	-0.00298
532	S_2	-0.00506	0.00131	-0.00114	0.00091	0.00249
481	S_3	0.00629	-0.00806	0.00288	-0.01540	-0.02061
271	S_4	0.00050	0.00138	-0.00065	0.00048	0.00015
265	S_5	-0.00839	0.00088	-0.00166	-0.00871	-0.01262

Table S50. Calculated values of electronic coupling for excitation energy transfer between the molecular units of the complex **amide2_edge**. The values in the matrix are total coupling (in eV). The letters in the grey cell refer to the molecular systems (see Figure S1) forming the studied complex.

VEE (nm) →		314	238	217	217	209
↓	↓C/H→	S_1	S_2	S_3	S_4	S_5
500	S_1	0.00236	-0.00425	-0.00204	0.00429	-0.00441
433	S_2	0.00950	-0.00046	0.00424	-0.00183	0.00300
360	S_3	-0.00312	0.00724	0.00844	-0.01360	0.01950
258	S_4	0.01247	-0.00204	0.00742	-0.00593	0.01249
247	S_5	-0.00071	0.00143	-0.00051	-0.00045	-0.00034

Table S51. Calculated values of electronic coupling for excitation energy transfer between the molecular units of the complex **amide3_core**. The values in the matrix are total coupling (in eV). The letters in the grey cell refer to the molecular systems (see Figure S1) forming the studied complex.

VEE (nm)	→	317	241	218	217	210
↓	↓B/H→	S_1	S_2	S_3	S_4	S_5
760	S_1	-0.00051	0.00122	-0.00030	0.00009	-0.00023
534	S_2	-0.00002	-0.00013	0.00065	0.00159	-0.00252
483	S_3	0.00410	-0.00615	0.00655	0.01400	-0.02220
272	S_4	0.00093	-0.00011	0.00007	-0.00006	0.00014
267	S_5	-0.00513	-0.00250	0.00026	-0.00107	0.00202

Table S52. Calculated values of electronic coupling for excitation energy transfer between the molecular units of the complex **amide3_edge**. The values in the matrix are total coupling (in eV). The letters in the grey cell refer to the molecular systems (see Figure S1) forming the studied complex.

VEE (nm)	→	317	241	218	217	209
↓	↓C/H→	S_1	S_2	S_3	S_4	S_5
506	S_1	-0.00180	0.00283	0.00386	-0.00859	0.01373
433	S_2	0.00261	0.00053	-0.00020	0.00003	-0.00100
360	S_3	-0.00519	0.00523	0.00577	-0.01326	0.02019
260	S_4	0.00425	0.00383	0.00328	-0.00613	0.00999
254	S_5	0.00170	-0.00672	-0.00451	0.00102	-0.00041

References

1   X. Shao, A. J. A. Aquino, M. Otyepka, D. Nachtigallová and H. Lischka, *Phys. Chem. Chem. Phys.*, 2020, **22**, 22003–22015.

2   H. Baba and M. Aoi, *J. Mol. Spectrosc.*, 1973, **46**, 214–222.

3   R. S. Becker, I. Sen Singh and E. A. Jackson, *J. Chem. Phys.*, 2004, **38**, 2144.

4   S. Shirai and S. Inagaki, *RSC Adv.*, 2020, **10**, 12988–12998.

5   S. Grimme and M. Waletzke, *J. Chem. Phys.*, 1999, **111**, 5645–5655.

6   C. Angeli, R. Cimiraglia and J. P. Malrieu, *Chem. Phys. Lett.*, 2001, **350**, 297–305.

7   C. Angeli, R. Cimiraglia and J. P. Malrieu, *J. Chem. Phys.*, 2002, **117**, 9138–9153.

8   B. Shi, D. Nachtigallová, A. J. A. Aquino, F. B. C. Machado and H. Lischka, *J. Chem. Phys.*, 2019, **150**, 124302.

9   V. Lukeš, M. Ilčin, J. Kollár, P. Hrdlovič and Š. Chmela, *Chem. Phys.*, 2010, **377**, 123–131.

10 A. Y. Freidzon, R. R. Valiev and A. A. Berezhnoy, *RSC Adv.*, 2014, **4**, 42054–42065.

11 M. Parac and S. Grimme, *Chem. Phys.*, 2003, **292**, 11–21.

12 A. Nakajima, *J. Lumin.*, 1977, **15**, 277–282.

13 E. A. Shirshin, G. S. Budylin, N. Y. Grechischeva, V. V. Fadeev and I. V. Perminova, *Photochem. Photobiol. Sci.*, 2016, **15**, 889–895.

14 D. S. Karpovich and G. J. Blanchard, *J. Phys. Chem.*, 1995, **99**, 3951–3958.

15 G. Basu Ray, I. Chakraborty and S. P. Moulik, *J. Colloid Interface Sci.*, 2006, **294**, 248–254.

16 E. L. Graef and J. B. L. Martins, *J. Mol. Model.*, 2019, **25**, 183.

17 C. K. Lin, *J. Comput. Chem.*, 2018, **39**, 1387–1397.

18 X. Niu, Y. Li, H. Shu and J. Wang, *Nanoscale*, 2016, **8**, 19376–19382.

19 S. Sarkar, M. Sudolská, M. Dubecký, C. J. Reckmeier, A. L. Rogach, R. Zbořil and M. Otyepka, *J. Phys. Chem. C*, 2016, **120**, 1303–1308.

20 M. Langer, T. Hrivnák, M. Medved' and M. Otyepka, *J. Phys. Chem. C*, 2021, **125**, 12140–12148.

21 T. Le Bahers, C. Adamo and I. Ciofini, *J. Chem. Theory Comput.*, 2011, **7**, 2498–2506.

22 C. Adamo, T. Le Bahers, M. Savarese, L. Wilbraham, G. García, R. Fukuda, M. Ehara, N. Rega and I. Ciofini, *Coord. Chem. Rev.*, 2015, **304**–**305**, 166–178.

23 D. Casanova and A. I. Krylov, *Phys. Chem. Chem. Phys.*, 2020, **22**, 4326–4342.

24 G. M. J. Barca, C. Bertoni, L. Carrington, D. Datta, N. De Silva, J. E. Deustua, D. G. Fedorov, J. R. Gour, A. O. Gunina, E. Guidez, T. Harville, S. Irle, J. Ivanic, K. Kowalski, S. S. Leang, H. Li, W. Li, J. J. Lutz, I. Magoulas, J. Mato, V. Mironov, H. Nakata, B. Q. Pham, P. Piecuch, D. Poole, S. R. Pruitt, A. P. Rendell, L. B. Roskop, K. Ruedenberg, T. Sattasathuchana, M. W. Schmidt, J. Shen, L. Slipchenko, M. Sosonkina, V. Sundriyal, A. Tiwari, J. L. Galvez Vallejo, B. Westheimer, M. Włoch, P. Xu, F. Zahariev and M. S. Gordon, *J. Chem. Phys.*, 2020, **152**, 154102.